Paleoceanography and Paleoclimatology®

AGU ADVANCING EARTH AND SPACE SCIENCE

RESEARCH ARTICLE
10.1029/2020PA004155

# Calcareous Nannofossil Size and Abundance Response to the Messinian Salinity Crisis Onset and Paleoenvironmental Dynamics

**A. M. Mancini[1,2], M. Grelaud[2], P. Ziveri[2,3], E. Nallino[1], and F. Lozar[1]**

[1]Department of Earth Sciences, Università degli Studi di Torino, Torino, Italy, [2]Institute of Environmental Science and Technology (ICTA), Universitat Autònoma de Barcelona (UAB), Bellaterra, Spain, [3]Catalan Institution for Research and Advanced Studies (ICREA), Barcelona, Spain

**Key Points:**

- High productivity and environmental instability drive calcareous nannofossil size toward the Messinian Salinity Crisis onset
- *Reticulofenestra minuta* size and mass respond to orbital-induced environmental dynamics
- The ongoing $pCO_2$ reduction characterizing the Messinian was not responsible for the recorded size variations

**Supporting Information:**

Supporting Information may be found in the online version of this article.

**Correspondence to:**

A. M. Mancini,
alanmaria.mancini@unito.it

**Citation:**

Mancini, A. M., Grelaud, M., Ziveri, P., Nallino, E., & Lozar, F. (2021). Calcareous nannofossil size and abundance response to the Messinian Salinity Crisis onset and paleoenvironmental dynamics. *Paleoceanography and Paleoclimatology*, *36*, e2020PA004155. https://doi.org/10.1029/2020PA004155

Received 27 OCT 2020
Accepted 20 AUG 2021



**Abstract** Dwarfism is a common feature affecting organisms across extreme events that characterized the Earth history, frequently referred as the result of "stressed conditions." To date, no study addressed the morphological and biometric changes across the Messinian Salinity Crisis (MSC), one of the most recent and impacting event occurred in the Mediterranean Sea, historically interpreted as characterized by hypersaline conditions. Here we focus on morpho/biometric changes affecting calcareous nannofossils (CN) toward the MSC onset in order to better constrain the paleoenvironmental dynamics and the loosely defined "stressed conditions" characterizing this interval. Size characterization and absolute abundance of selected CN taxa were performed in the Perales (Spain, Western Mediterranean) and in the Banengo and Pollenzo sections (Italy, Northern Mediterranean). We also tested whether size changes and orbital cyclicity were related through analyzing size and calcite mass of *Reticulofenestra minuta* using an automated image analysis system of CN recognition (SYRACO). We recorded a significant size reduction affecting the CN taxa involved in the MSC onset bioevent, related to the restriction of the Mediterranean Basin that resulted in increased productivity and enhanced environmental variability, stimulating CN growth rate and decreasing their platelet sizes. *Reticulofenestra minuta* size and mass correlate with the orbital cyclicity with minimum values during periods of enhanced environmental variability, coinciding with the diatomite deposition in the Sorbas Basin. Our finding reveals that the size change recorded across the MSC onset coincided with the instauration of a productive and highly variable environment, linked to the restriction of the paleo Gibraltar Strait.

## 1. Introduction

Calcareous nannofossils (CN) are the remaining of calcifying marine algae (coccolithophores) and *incertae sedis* species producing small calcite platelets that are usually well preserved in the fossil record. The coccolithophores remains represent a powerful tool to document past environmental variability through the study of their assemblages (e.g., Negri et al., 1999), their morphologic features (e.g., Faucher et al., 2020; Grelaud et al., 2012), or the stable isotope/trace elements of their calcite (e.g., Bolton et al., 2016: Dedert et al., 2014; Stoll et al., 2019). Previous studies addressed the coccolithophores response to major environmental changes in the world ocean, both in the past (e.g., during Oceanic Anoxic Events) (Browning & Watkins, 2008; Erba et al., 2010; Lübke et al., 2015) and in the present (e.g., anthropogenic climate change) (Milner et al., 2016; Zondervan, 2007 and references therein), revealing that the coccolithophores responded to these perturbations by drastic changes in their specific diversity, their total abundances and the morphology and mass of their platelets (Meier et al., 2014). Sea temperature, salinity, nutrients content, light intensity, trace metals or carbonate chemistry (e.g., $pCO_2$) changes are proven to impact the size of coccolithophore cells and their calcitic platelets (Beaufort et al., 2011; Bollmann & Herrle, 2007; Paasche, 2002; Watabe & Wilbur, 1966; Zondervan, 2007). Of particular interest is the impact of past (e.g., Beaufort et al., 2011) and current (anthropogenic) (de Bodt et al., 2010; Engel et al., 2005; Langer et al., 2006; Riebesell et al., 2000, 2016; Zondervan, 2007) increase in $pCO_2$ on the coccolithophores affecting their major role on the oceanic carbon budget and carbonate pump (Rost & Riebesell, 2004; Salter et al., 2014).

Mesocosm and laboratory culture studies (e.g., D'Amario et al., 2020; Langer et al., 2011; Meyer & Riebesell, 2015; Oviedo et al., 2015; Sheward et al., 2017; Triantaphyllou et al., 2018; Ziveri et al., 2014;

Zondervan, 2007) highlight coccolithophores sensitivity to changes in abiotic parameters affecting their CN plate morphometry. Consequently, applying the outcome from modern studies, the CN morphological study can be used as a proxy to reconstruct past environmental conditions (Faucher et al., 2020; Gibbs et al., 2013 and references therein).

Marine biota frequently responded to extreme events such as greenhouse warming, eutrophication and volcanic events showing an overall size reduction (Erba et al., 2010; Ferreira et al., 2017; Keller & Abramovich, 2009; Lübke et al., 2015; Mattioli et al., 2009; Salaviale et al., 2018; Tremolada et al., 2008). Also, minor environmental changes such as the shallowing/shrinkage of the basin, were documented to impact the size of marine biota (Keller & Abramovich, 2009). Overall, the marine biota size decrease is related to variation in the oxygen, salinity and nutrients contents as well as change in temperature (Keller & Abramovich, 2009). This biotic response to such events is referred as "Lilliput effect" (Urbanek, 1993), and accompanied for instance the Oceanic Anoxic Events (Erba et al., 2010) and mass extinction episodes, but was also recorded in other time intervals characterized by environmental conditions loosely defined as "stressed condition" (Ferreira et al., 2017; Violanti et al., 2013). Although the CN morphometry and its relations with the environmental parameter was explored in modern environment and during extreme event characterizing the Earth history, no study addressed the impact of one of the most recent and rapid events affecting the Mediterranean: the Messinian Salinity Crisis (MSC).

During the Messinian, the Mediterranean Basin was affected by climatic and tectonic instability, resulted in the progressive restriction of the basin (Flecker et al., 2015) that culminated in the deposition of a huge amount of evaporite, started at 5.97 Ma (Manzi et al., 2013). The precipitation of the 6% of the late Miocene ocean NaCl (1 million of $Km^3$; Blanc, 2006) testifies the dramatic nature of this event, that likely contributed to the decline of $pCO_2$ characterizing the late Miocene, through change in the Mediterranean-Atlantic exchanges and consequently on the world ocean circulation (Capella et al., 2019). Calcareous nannoplankton were sensitive to the changing environment characterizing the MSC onset; in fact, a peculiar fossil signal was recognized at the Mediterranean basin scale approximating the MSC onset (Lozar & Negri, 2019; Lozar et al., 2018; Mancini et al., 2020). This fossil signal was first identified by Lozar et al. (2018) and described as a succession of peak in abundance of the taxa *Sphenolithus abies*, followed by *Helicosphaera carteri*, *Umbilicosphaera rotula*, and *Rhabdosphaera clavigera*. This event, previously recognized in the Piedmont Basin, in the Northern Apennines and in the Eastern Mediterranean (Lozar & Negri, 2019), was recently recorded also in the Westernmost Messinian basin (i.e., the Sorbas Basin) and referred as MSC onset bioevent; it marks the last restriction step affecting the Mediterranean-Atlantic water exchange, resulting in an increase in the sensitivity of the Mediterranean basin to external forcing (Mancini et al., 2020).

The present study focuses on the impact of the MSC on CN morphometry through biometric analyses performed on selected CN taxa, with the aim to explore if CN morphometry changes accompanied this event and to constrain the paleoenvironmental meaning of these morphological variations. Samples were collected in the Sorbas Basin, which is one of the best constrained basins from a chronostratigraphic and paleoenvironmental perspective (Baggley, 2000; Clauzon et al., 2015; Filippelli et al., 2003; Flores et al., 2005; MartÍn et al., 2004; Mancini et al., 2020; Modestou et al., 2017; Pérez-Folgado et al., 2003; Reghizzi et al., 2017; Sierro et al., 2001, 2003; Troelstra et al., 1980). In order to demonstrate that the recorded size change does not represent a stochastic or local response, samples from the Piedmont Basin were analyzed and compared with Sorbas Basin samples.

We also discuss the main drivers of the recorded size fluctuation in order to better constrain the loosely defined environmental "stressed conditions" affecting the Mediterranean Sea before and during the MSC, often thought to be the result of hypersaline conditions in the water column.

We also test if the CN size fluctuations are related to orbital forcing, known to modulate the overall abundances of the microfossil assemblages and the deposition of lithological quadripartite cycle in the Sorbas basin (Mancini et al., 2020; Sierro et al., 2003), by analyzing the taxa *Reticulofenestra minuta* at high resolution using SYRACO, an automated system of coccoliths recognition and measurements (Beaufort & Dollfus, 2004).

The possible effects on the CN biometry of the decreasing $pCO_2$ trend characterizing the Messinian is also discussed.

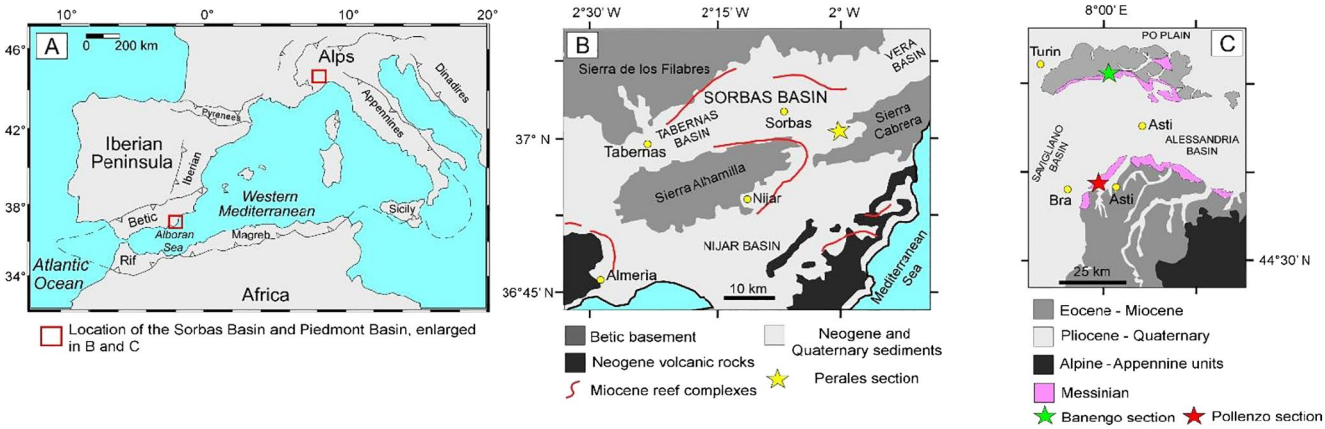


**Figure 1.** (a) Location of the Sorbas Basin in the western Mediterranean Sea (modified from Corbí and Soria [2016]). (b) Geological map of South-East Spain showing the Sorbas Basin and the Perales section (modified from Bourillot et al. [2009]). (c) Geological map of the North-West Italy showing the Piedmont Basin and the Banengo and Pollenzo sections (modified from Natalicchio et al. [2019] and Sabino et al. [2020]).

## 2. Material and Methods

### 2.1. Studied Material and Age Model

Samples were collected in the Perales section (37° 05′ 49″N, 2° 03′ 19″W, Sorbas Basin, S-E Spain; Figures 1a and 1b) spanning a time interval from ≃6.23 to 5.97 Ma (11 precessional cycles) retrieved from ≃23 m of outcropping succession. At least six samples were collected for each precessional cycle, for a total of 116 samples. The pre-evaporitic Sorbas Basin deposits belong to the upper member of the Abad marls (UA) and consist of precession driven quadripartite sedimentary cycles, each consisting of an alternation of sapropel and diatomite layers that are intercalated between homogeneous white marls (Sierro et al., 2001, 2003). The age model was built based on foraminifer bioevents (Mancini et al., 2020; Sierro et al., 2001) and on the recognition of the first gypsum layer, marking the MSC onset in the Sorbas Basin (Mancini et al., 2020; Manzi et al., 2013). In the Piedmont Basin, six sample were studied spanning the last five pre-evaporitic precessional cycle in the Banengo section (45° 04′21″N, 8° 03′23″E; Figures 1a and 1c) and nine samples spanning the last seven pre-evaporitic precessional cycle in the Pollenzo section (44° 41′06″N, 7° 55′29″E). In the Piedmont Basin, the precessional cyclicity in the pre-evaporitic successions is defined by the alternation of shale (sapropel equivalent) and white marls/carbonate rich layers (Dela Pierre et al., 2011; Lozar et al., 2018). The age model relies on foraminifer bioevents (Lozar et al., 2018; Violanti et al., 2013) and the recognition of the first branching selenite bed, that corresponds to the sixth precessional cycle of the first stage of the MSC (Dela Pierre et al., 2011; Lugli et al., 2010).

### 2.2. Absolute Abundance: Samples Preparation and Counting

In order to perform the absolute abundance analyses, samples were prepared following the protocol developed by Beaufort et al. (2014). Briefly, a small amount of dried sediment (≃2.0 mg) was disaggregated into a 50 ml tube using a micro spoon. The tube was filled with ELIX water until 45 ml, hand mixed and sonicated for few seconds (≅2 s). A constant volume of the suspension (7 ml) was extracted with a pipette, poured into a beaker and sonicated a second time (≃2 s). The solution was then transferred, the beaker being cleaned 3 times by spraying ELIX water, into a petri dish with a cover slide at the bottom and left to settle for 4 h. After the sedimentation of the material, the water was evaporated in an oven at 70°C. The obtained samples were permanently mounted on a slide with Norland Optical Adhesive 61 (“NOA61”) and analyzed through light microscopy.

In each sample, a minimum of 500 nannofossils were identified using Olympus BX51 polarized microscope and counted at 1250X magnification. The reworked specimens, whose stratigraphic range is older than that of the analyzed material, were not included in the counting but they were counted separately. The final results are expressed in number of nannofossils per gram of dried sediment (CN/g).

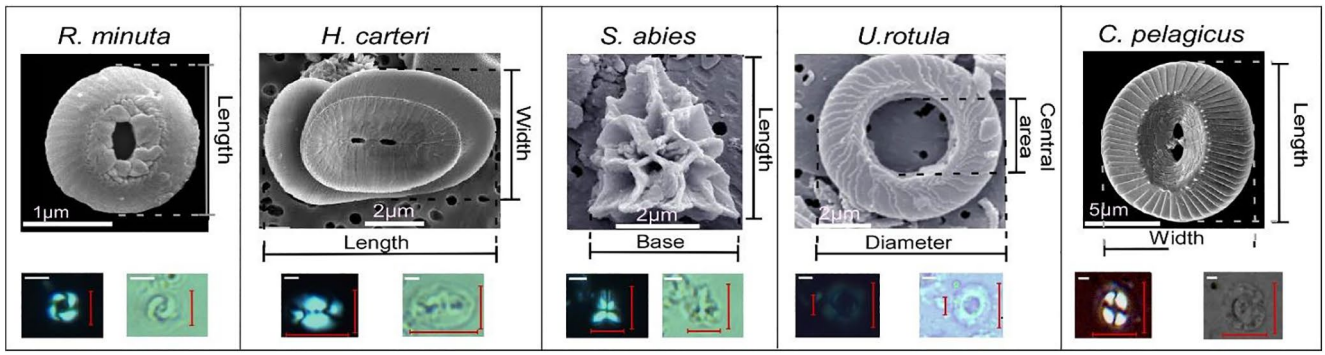


**Figure 2.** Electron microscope photographs of the calcareous nannofossil object of this study with the measured morphometrical parameters at the electronic microscope (above) and at the light microscope (below; the red lines represent the measured biometric parameter; scale bar is 2 µm). The electronic microscope pictures have been redrawn and modified from Nannotax3 website (http://www.mikrotax.org/Nannotax3) (courtesy of Young et al. [2017]).

### 2.3. Biometric Measurements

One of the major issues in the biometric studies is the preservation of the specimens under exam, therefore we performed biometric measurements only on the well preserved specimens (see Supporting Information S1 for details); the broken, overgrown and etched specimens were excluded from the measurements following the common practice in this kind of study (Faucher, Erba, et al., 2017; Herrmann & Thierstein, 2012; Herrmann et al., 2012; Lübke & Mutterlose, 2016; Mattioli et al., 2004, 2009; Suchéras-Marx et al., 2010). For each selected sample, the morphological parameters (Figure 2) of 50 specimens were measured, that represents the common number used among the CN biometric studies (Faucher, Erba, et al., 2017; Lübke & Mutterlose, 2016; Tremolada et al., 2008). The number of analyzed samples depended on the abundance of the analyzed taxa and the overall preservation of the assemblage; measurements were performed in 24 samples for *S. abies*, in 34 samples for *H. carteri*, in 26 samples for *U. rotula* and in 32 for *Coccolithus pelagicus*. Pictures of the specimens were obtained from a Jenoptik camera (using Progres 5 software) mounted onto Olympus BX50 microscope with a magnification of 1250X. The pictures were analyzed with the software ProGres 5. At least 1–2 samples were analyzed for each precessional cycle (from UA23 to UA33), except in the last pre-evaporitic cycle (UA34) where all samples containing the selected CN taxa were analyzed. This has been done in order to reveal the biometric change accompanying the MSC onset bioevent and the MSC onset.

Regarding *S. abies*, the measures were taken with the specimens viewed at 45° to the polarizers in order to discern the apical spine length. For *H. carteri* and *C. pelagicus*, the ellipticity index (average length/average width) was calculated in order to highlight morphometric changes. In our study the ellipticity index is used to track eventual malformations affecting nannofossils, evaluating the deviation from the ellipticity average calculated in our data set. In the Perales section, for *U. rotula*, both the coccolith external and central area diameters (Figure 2) were measured. The ratio between central area diameter/total diameter lengths were calculated and values close to one indicate a large central area over the total diameter.

In order to demonstrate that the morphometric change accompanying the MSC onset bioevent were global or coeval, size analyses were performed in Banengo and Pollenzo sections (Piedmont basin, North Mediterranean) as well. The samples were analyzed following the procedure described above. In Banengo section six samples were analyzed (1 for each precessional cycle) for *S. abies* and *H. carteri*; in Pollenzo section nine samples were analyzed (1–2 for each precessional cycle) for *S. abies* and *H. carteri*. *Coccolithus pelagicus* and *U. rotula* were not analyzed in the Piedmont Basin because their lower abundance and poorer preservation.

### 2.4. SYRACO: Corrected Length and Calcification Index

SYRACO is an automated system of coccoliths recognition developed by Beaufort and Dollfus (2004). In our study, SYRACO was used for the recognition and the measurement of the length and the mass of *R. minuta* coccolith; data collection was performed at the Universitat Autònoma de Barcelona (UAB) during spring 2018. This analysis was performed on *R. minuta*, the only taxon present in all the analyzed samples, from

the Perales section which is precession controlled and spans a long enough time interval. This makes possible the comparison of long term morphometry changes to the paleoenvironmental context associated with precessional fluctuation in the Perales section, which is well constrained by previous studies (Baggley, 2000; Clauzon et al., 2015; Filippelli et al., 2003; Flores et al., 2005; Mancini et al., 2020; MartÍn et al., 2004; Modestu et al., 2017; Pérez-Folgado et al., 2003; Reghizzi et al., 2017; Sierro et al., 2001, 2003; Troelstra et al., 1980). A certain amount of pictures (at least 40, depending on the abundance of *R. minuta*) were taken with a SPOT insight camera mounted on a LEICA 6000B microscope with a X1000 magnification. A total of 97 samples were processed and a minimum of 200 *R. minuta* coccoliths were measured by SYRACO for each sample. In order to test the reliability of the SYRACO measures, 10 samples were selected for comparing the SYRACO results with a classical manual measurement at the light microscope. In each sample 100 *R. minuta* were identified and measured using the software ProGres 5. The obtained average values were successively processed in order to obtain the equation of the linear regression between SYRACO and the manual measurements (Figure 3a). The linear regression equation was successively used to correct the SYRACO-derived length in all the remaining samples (Figure 2a). In order to have a comparable data set, we used only the SYRACO measurements for the doubled measured parameters.

*Reticulofenestra minuta* calcification index was obtained following the protocol developed by D'Amario et al. (2018); dividing the mass values obtained from SYRACO by the normalized mass (density of calcite × coccolith volume). To calculate the coccolith volume, we multiplied the cube of the corrected length by $K_s$ (estimated shape dependent constant). Unfortunately, the $K_s$ values for *R. minuta* was never calculated (Young & Ziveri, 2000), so we choose to use the $K_s$ calculated for *Gephyrocapsa oceanica* (0.05) that approximate the shape of *R. minuta*.

### 2.5. Statistical Analysis

All the statistic treatments were performed using the software Past 4.03 (Hammer et al., 2001) and Excel. For each selected species, the average of the morphometric parameters, the deviation from the mean average (expressed in %), as well as the standard deviation were calculated. One-way ANOVA (parametric ANalysis Of VAriance) test were performed in order to assess the degree of variance between the obtained means. The null hypothesis is that all the obtained means are the same and the encountered differences among the means are stochastic and not significant. In the case that ANOVA revealed significant differences ($p < 0.05$), a post-hoc Tukey HSD (Honestly Significant Difference) test was performed in order to identify which of the samples (or group of samples belonging to the same precessional cycle) differed. The correlation coefficient $R^2$ was calculated between the measured biometric parameters for all the analyzed taxa in the three analyzed sections. Finally, frequency histograms were performed for all the analyzed taxa in order to assess which size class is more common in our data set.

## 3. Results

Calcareous nannofossils are abundant and moderately/well preserved within the study interval and sections (for detail see Figure S1). The ANOVA test results recorded a significant size variation affecting our data set in all the section studied for all the taxa considered. The Tukey HSD test identified where are located the samples and cycles which statistically differed (for detail see Figures S2 and S3). The target taxa concentration and morphometric data are shown in Table 1 and Figures 3–8 with key trends noted below.

### 3.1. *Helicosphaera carteri*

In the Perales section, *H. carteri* absolute abundances never exceed $0.40 \times 10^9$ CN/g, except in the cycles UA23, UA32, and UA34, where absolutes abundances from $0.55 \times 10^9$ to $1.35 \times 10^9$ CN/g were recorded (Figure 4). *Helicosphaera carteri* length and width range from a minimum of 4.7 and 3.4 μm respectively, to a maximum of 11.0 and 7.9 μm (Figure 3c) respectively. The average size of *H. carteri* shows maxima values in a cluster of samples in the cycle UA29; minima values are reached in the cycle UA34, where a statistically significant decrease from the mean average was recorded (Figures 4 and S2). The ellipticity index show higher values preferentially when the *H. carteri* width is below the average size. Highest ellipticity index values were recorded in the cycles UA23, UA24, UA26, and UA34 (Figure 4). In the Banengo

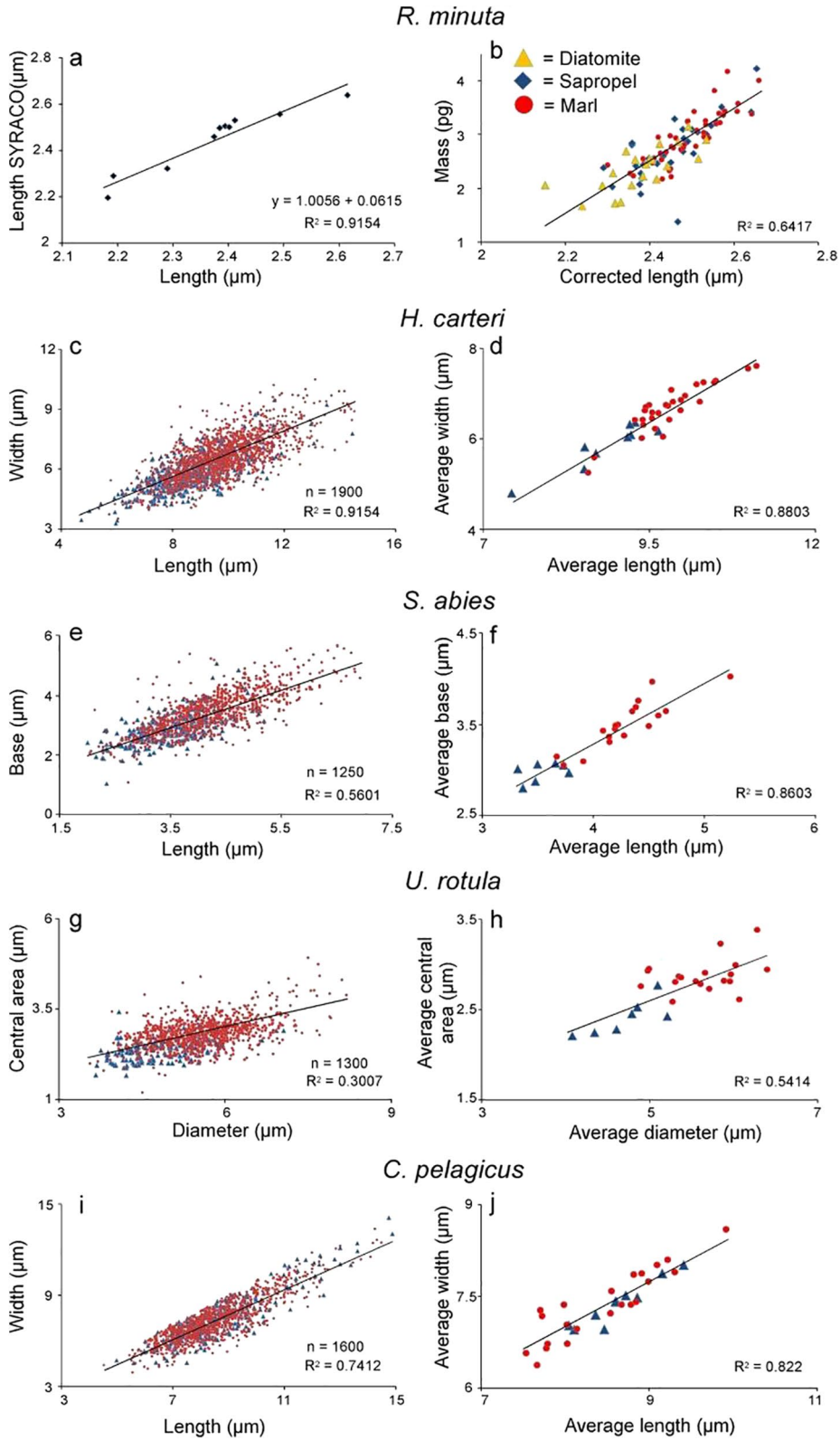
R. minuta
a
Length SYRACO(µm)
y = 1.0056 + 0.0615
R² = 0.9154
Length (µm)
b
= Diatomite
= Sapropel
= Marl
Mass (pg)
R² = 0.6417
Corrected length (µm)
H. carteri
c
Width (µm)
n = 1900
R² = 0.9154
Length (µm)
d
Average width (µm)
R² = 0.8803
Average length (µm)
S. abies
e
Base (µm)
n = 1250
R² = 0.5601
Length (µm)
f
Average base (µm)
R² = 0.8603
Average length (µm)
U. rotula
g
Central area (µm)
n = 1300
R² = 0.3007
Diameter (µm)
h
Average central area (µm)
R² = 0.5414
Average diameter (µm)
C. pelagicus
i
Width (µm)
n = 1600
R² = 0.7412
Length (µm)
j
Average width (µm)
R² = 0.822
Average length (µm)

**Figure 3.**

**Table 1**
*Mean Average Value Expressed in μm (*Except the Mass, That is Expressed in pg) of the Measured Biometric Parameter With the Calculated Standard Deviation for Every Taxa Analyzed in the Different Section*

| | *H. carteri* | | *S. abies* | | *U. rotula* | | *C. pelagicus* | | *R. minuta* | |
|---|---|---|---|---|---|---|---|---|---|---|
| | Length | Width | Length | Base | Diameter | Central area | Length | Width | Length | *Mass (pg) |
| Perales | 9.57 ± 1.48 | 6.47 ± 0.91 | 4.10 ± 0.74 | 3.37 ± 0.61 | 5.39 ± 0.65 | 2.7 ± 0.32 | 9.5 ± 1.47 | 7.3 ± 1.39 | 2.45 ± 0.09 | 2.76 ± 0.54 |
| Pollenzo | 7.79 ± 1.30 | 4.89 ± 0.75 | 4.08 ± 0.79 | 3.51 ± 0.63 | / | / | / | / | / | / |
| Banengo | 8.99 ± 1.09 | 5.80 ± 0.73 | 4.16 ± 0.71 | 3.59 ± 0.58 | / | / | / | / | / | / |

section, *H. carteri* length and width span from 6.1 to 12.1 μm and from 4.2 to 7.3 μm respectively (Figure 5). The minimum average *H. carteri* size values are recorded during the MSC onset bioevent in concomitance with *H. carteri* peak in relative abundance (Figure 6); the ellipticity index shows highest values in the cycles Bm2 and Bm5. In the Pollenzo section *H. carteri* length and width span from 4.27 to 11.7 μm and from 2.5 and 6.5 μm respectively (Figure 5). The minimum *H. carteri* size value is recorded during the MSC onset bioevent in concomitance with *H. carteri* peak in relative abundance (Figure 6), although sizes below the mean average were documented also in the 2 cycles before (UA32 and UA33) the MSC onset bioevent. In the Pollenzo section, after the MSC onset bioevent, *H. carteri* partially recovered its mean size which remains below the average mean size calculated in this site. The ellipticity index in the Pollenzo section shows an opposite trend compared to the other section, with minimum values during the MSC onset bioevent. Some differences emerged comparing the correlation coefficient (i.e., $R^2$), between the measured length, width and the ellipticity index (Figures 3, 5, and S4). The correlation coefficient between length and width was higher in Perales section ($R^2 = 0.9154$) than in the Banengo ($R^2 = 0.5608$) and Pollenzo ($R^2 = 0.6731$) sections. These differences could be the results of the different amount of sample analyzed and specimens measured. Furthermore, the analyzed time interval in the two sections of the Piedmont Basin contain few precessional cycle before the MSC onset, which were characterized by unstable environmental conditions, likely resulting in a more variability of the measured biometric parameters.

### 3.2. *Sphenolithus abies*

In the Perales section, *S. abies* absolute abundance never exceeds the $0.5 \times 10^9$ CN/g, except in the cycle UA34 where the highest abundances are recorded (from $2.06 \times 10^9$ to $3.45 \times 10^9$ CN/g). As already observed for *H. carteri*, the 2 measured parameters (base and length) tend to increase together although this relation seems to be less marked for *S. abies* ($R^2 = 0.5601$). *Sphenolithus abies* length and base span from 2.3 to 6.9 μm and 1.0–5.7 μm, respectively (Figure 3e). The averages of *S. abies* lengths and base in the cycle UA34 show statistically significant decrease (Figures 4, S2, S3, and S5). More generally, a decreasing trend of the measured parameters is discernible from the cycle UA29 (where the maxima values are recorded) upward (Figure 4).

In the Banengo section *S. abies* base and length span from 1.8 to 5.9 μm and 2.5–6.2 μm, respectively (Figure 5). It shows a decreasing trend of the average basal width from the bottom to the top (Figure 6). The minimum *S. abies* average value is recorded during the MSC onset bioevent, matching the *S. abies* peak in relative abundance (Figure 6).

In the Pollenzo section *S. abies* length and base span from 1.5 to 6.5 μm and 1.7–6.5 μm, respectively (Figure 5); the minimum average value is recorded during the MSC onset bioevent, matching the *S. abies* peak

**Figure 3.** Relationship between the morphometrical parameters measured for each calcareous nannofossil taxa (Perales section, Sorbas Basin). (a) Relationship between the average *R. minuta* length obtained using SYRACO and with an operator. The obtained linear regression equation has been successively used to correct the data obtained from SYRACO (see Section 2.4). (b) Relationship between the average *R. minuta* corrected length and the average mass for each lithology of the Perales section. The $R^2$ value was calculated considering the entire data set (triangle + cycle + diamond). (c, e, g, and i) Relationship between the morphometrical parameters for each selected taxa, where n is the number of measured calcareous nannofossil, the blue triangles represent the size during the MSC-CN bioevent and the red cycles the size in the remaining part of the section. The $R^2$ value was calculated considering the entire data set (triangle + circle). (d, f, h, and j) Relationship between the average length or diameter and the average width, base or central area. Blue triangles mark the calcareous nannofossil average size during the MSC-CN bioevent, the red circles the average size in the remaining part of the section. The $R^2$ value was calculated considering the entire data set (triangle + circle).

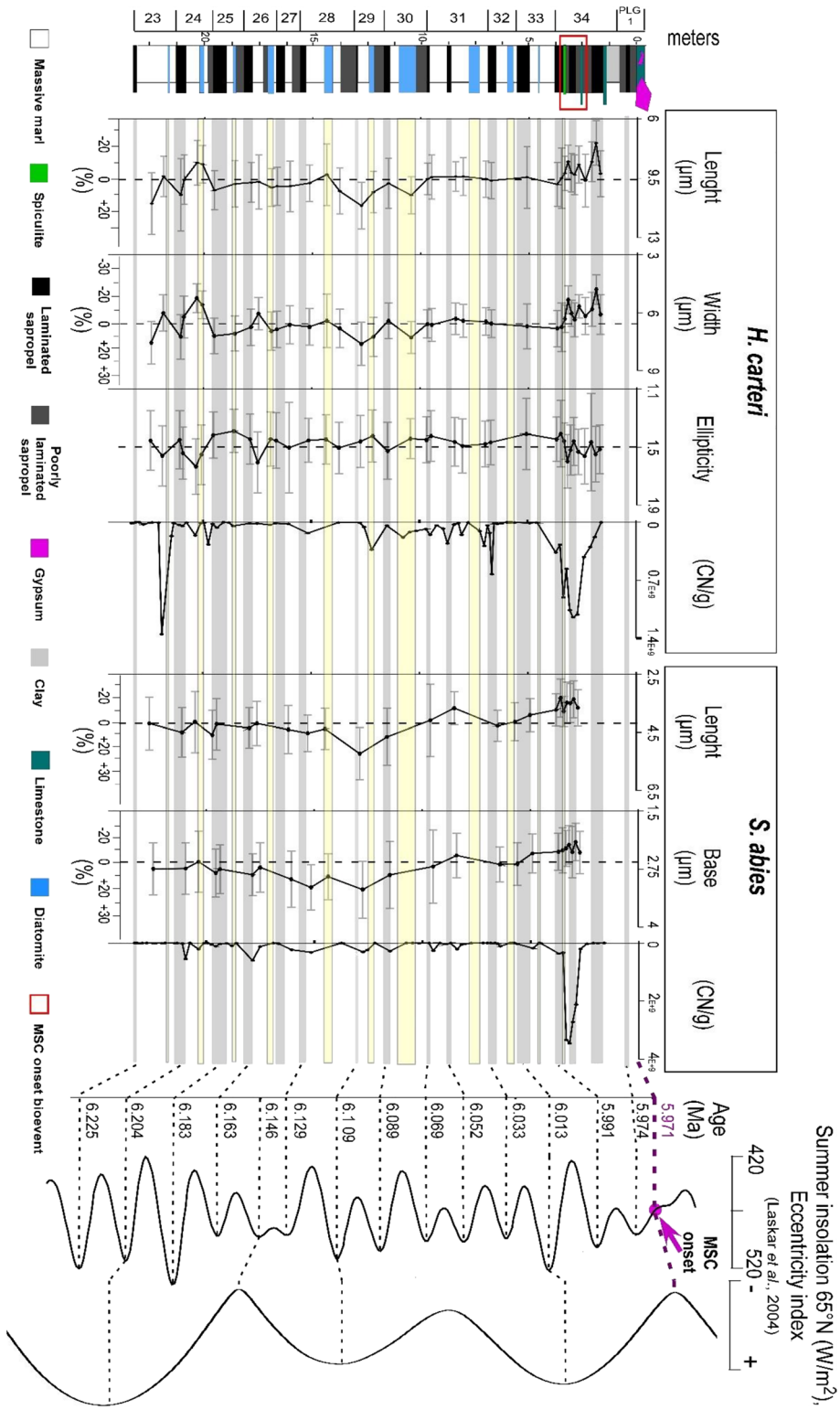


**Figure 4.** *Helicosphaera carteri* and *S. abies* biometric measurements and absolute abundances in the Perales section compared with the change in orbital parameters (precession and eccentricity from Laskar et al. [2004]). The error bars represent the standard deviation. The dashed line represents the mean average, the lower axis shows the variation expressed in % from the mean average. The red rectangle indicates the position of the Messinian Salinity Crisis onset bioevent (Mancini et al., 2020).

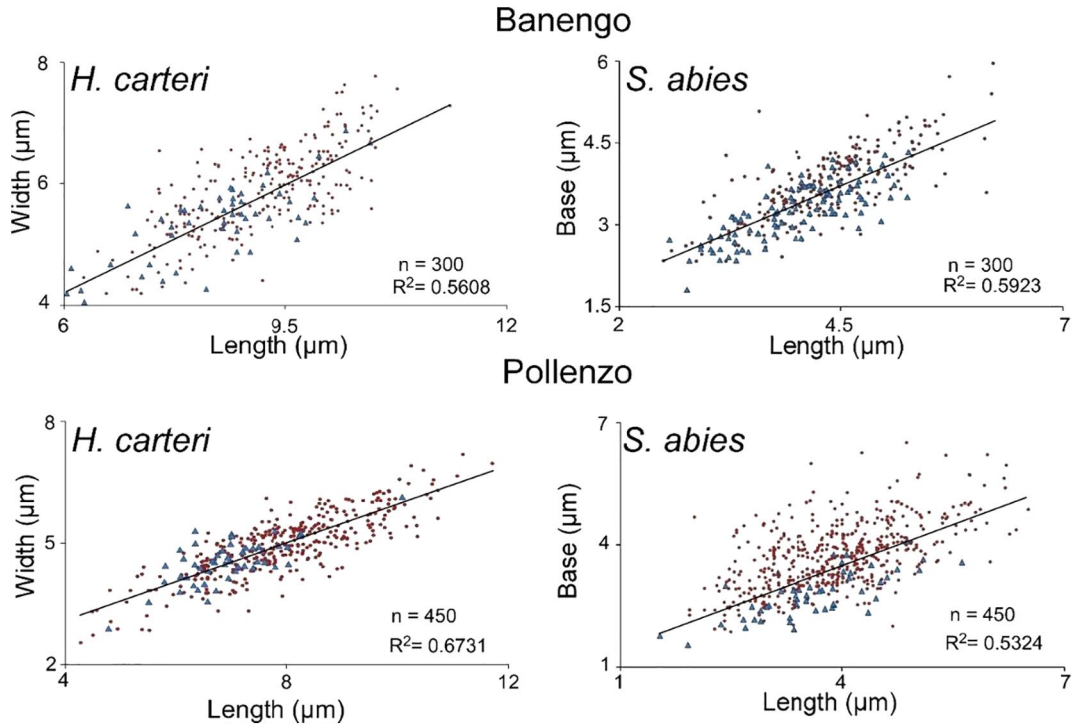


**Figure 5.** Relationship between the morphometrical parameters measured for *H. carteri* and *S. abies* (Banengo and Pollenzo sections, Piedmont Basin), where n is the number of measured coccoliths, the blue triangles represent the size during the MSC-CN bioevent and the red circles the size in the remaining part of the section. The $R^2$ value was calculated considering the entire data set (triangle + circle).

in relative abundance (Figure 6). Above the MSC onset bioevent, *S. abies* shows size values below the average calculated in this site.

### 3.3. *Umbilicosphaera rotula*

Due to the rarity and poor preservation of *U. rotula* in the Piedmont Basin, it has only been possible to measure it consistently throughout the Perales section.

In the Perales section, *U. rotula* absolute abundance never exceed the $0.2 \times 10^9$ CN/g, except in the cycle UA24 ($0.37 \times 10^9$ CN/g) and in the cycle UA34, where its maximum abundance was reached ($1.12 \times 10^9$ CN/g) (Figure 7). *Umbilicosphaera rotula* diameter and central area size span from a minimum 3.2 and 1.2 µm, to a maximum of 8.3 and 4.1 µm respectively (Figure 3g). We found a large morphometric variability in *U. rotula*, with specimens showing heterogeneous central area/diameter index (Figure 7). High *U. rotula* diameter size is recorded in the cycles UA23, UA28 and UA29; the lowest *U. rotula* diameter size is recorded in the cycle UA34, where a statistically significant decrease from the average recorded (Figures 7 and S2). Likewise the *S. abies* trend, a general decreasing trend of the *U. rotula* diameter is recognizable from UA29 onward with the exception of UA32 where an increase in the diameter is observed. *Umbilicosphaera rotula* central area measurements show high values in the cycle UA23 and UA28, whereas minimum values are recorded in the cycle UA34.

### 3.4. *Coccolithus pelagicus*

In the Perales section, *C. pelagicus* absolute abundance is generally low (below $2.5 \times 10^8$ CN/g), with the exception of cycle UA34 where it increases up to $8.72 \times 10^8$ CN/g (Figure 7). *Coccolithus pelagicus* length and width span from a minimum of 4.3 and 3.8 µm respectively, to a maximum of 14.3 and 13.4 µm respectively (Figure 3i). The ellipticity index does not mark any significant variation, and slightly fluctuates close to the mean average (Figure 7). The length and the width trends are well correlated ($R^2 = 0.7412$, Figure 3i),

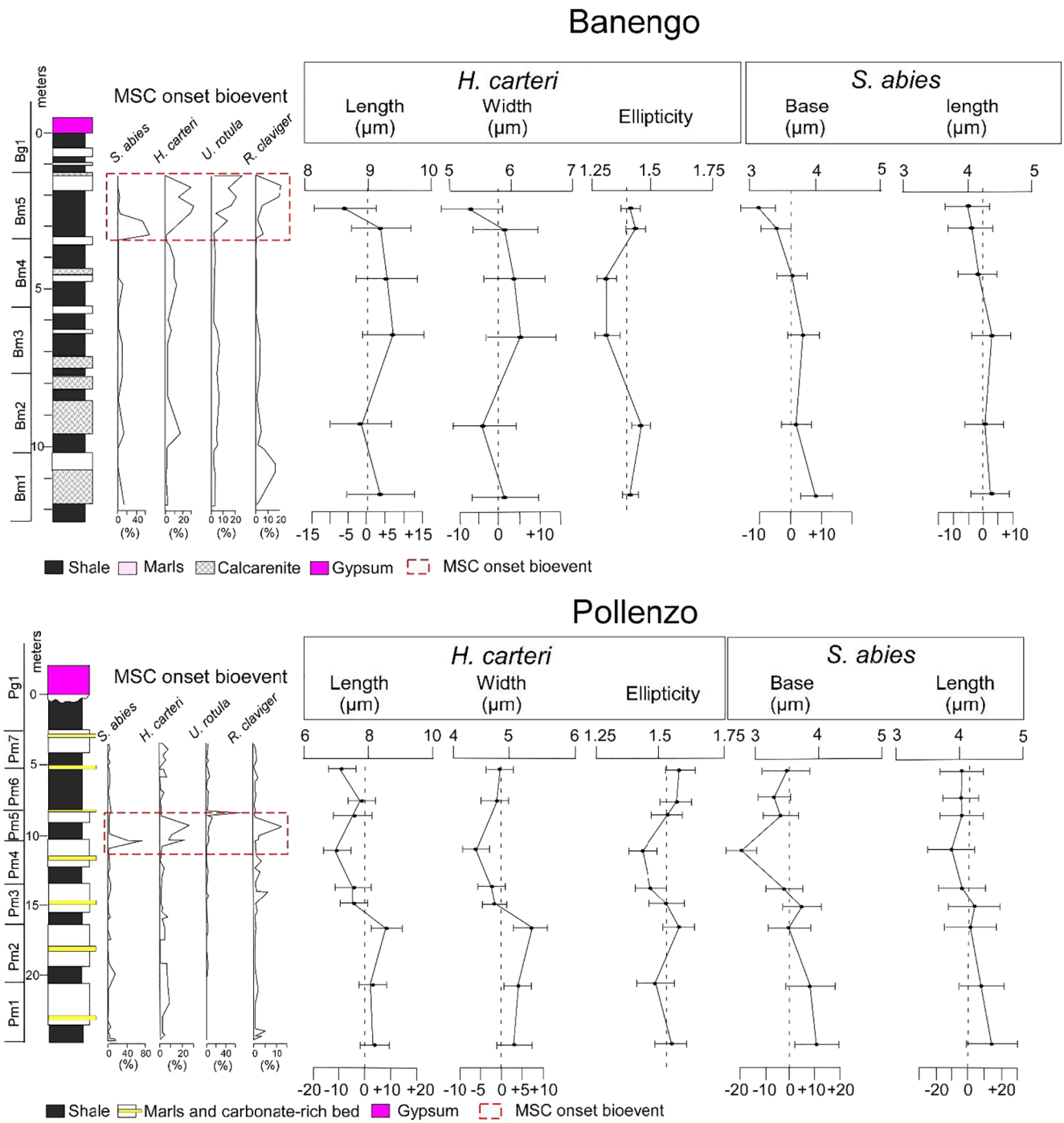


**Figure 6.** *Helicosphaera carteri* and *S. abies* biometric measurements in the Banengo and Pollenzo sections (Piedmont Basin) compared with the relative abundance of the species involved in the Messinian Salinity Crisis onset bioevent. The error bars represent the standard deviation. The dashed line represents the mean average, the lower axis shows the variation expressed in % from the mean average.

showing maxima values from the bottom up to the cycle UA26. A slight increase in *C. pelagicus* length and width is also recognizable in the cycle UA34 (Figure 7). Differently from the others analyzed taxa, *C. pelagicus* does not show a size reduction in the UA34 but it retains size values that fluctuate around the mean average.

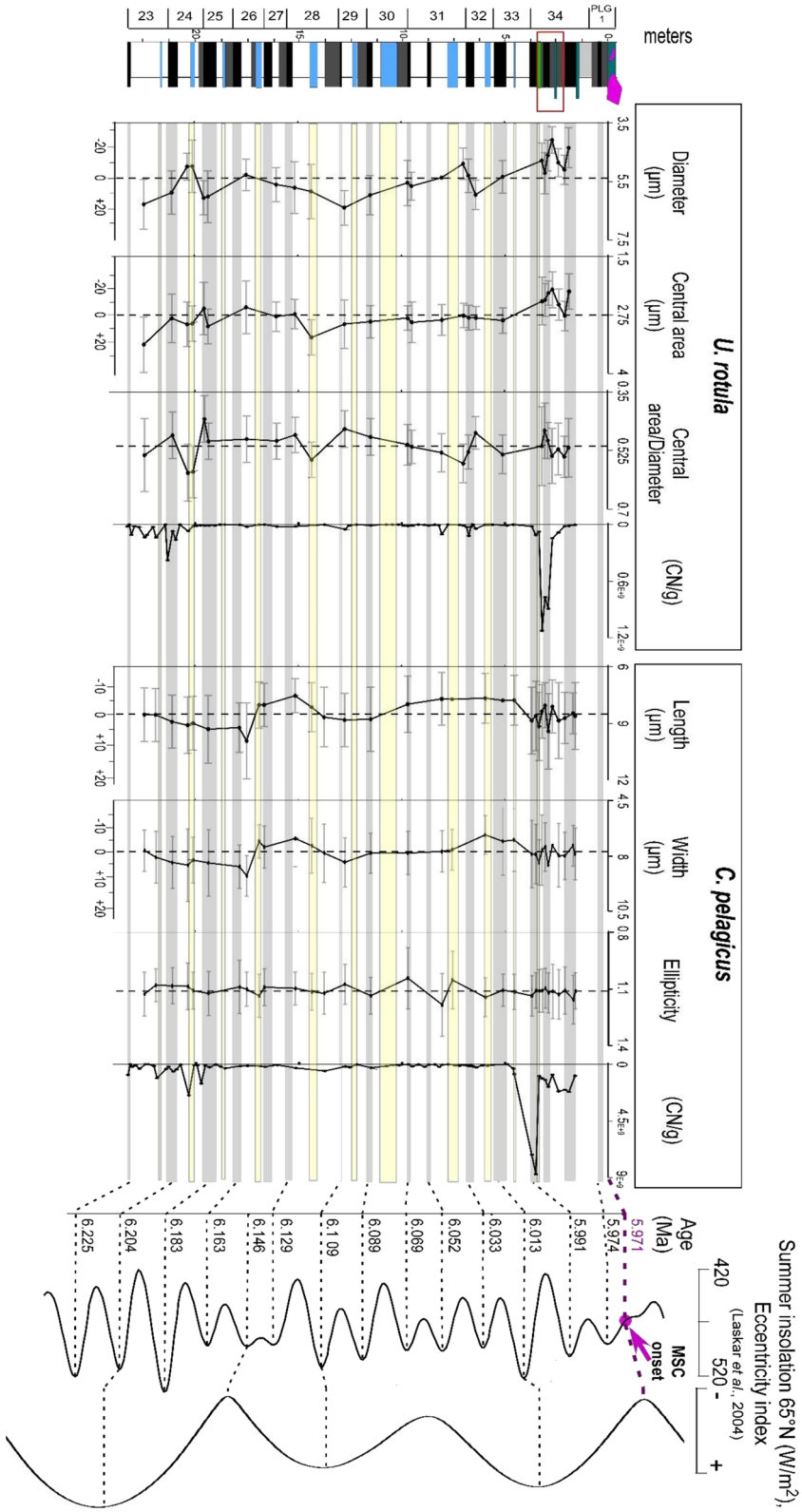


**Figure 7.** *Umbilicosphaera rotula* and *C. pelagicus* biometric measurements and absolute abundances in the Perales section compared with the change in orbital parameters (precession and eccentricity from Laskar et al. [2004]). The error bars represent the standard deviation. The dashed line represents the mean average, the lower axis shows the variation expressed in % from the mean average. The red rectangle indicates the position of the Messinian Salinity Crisis onset bioevent (Mancini et al., 2020). Legend as in Figure 4.

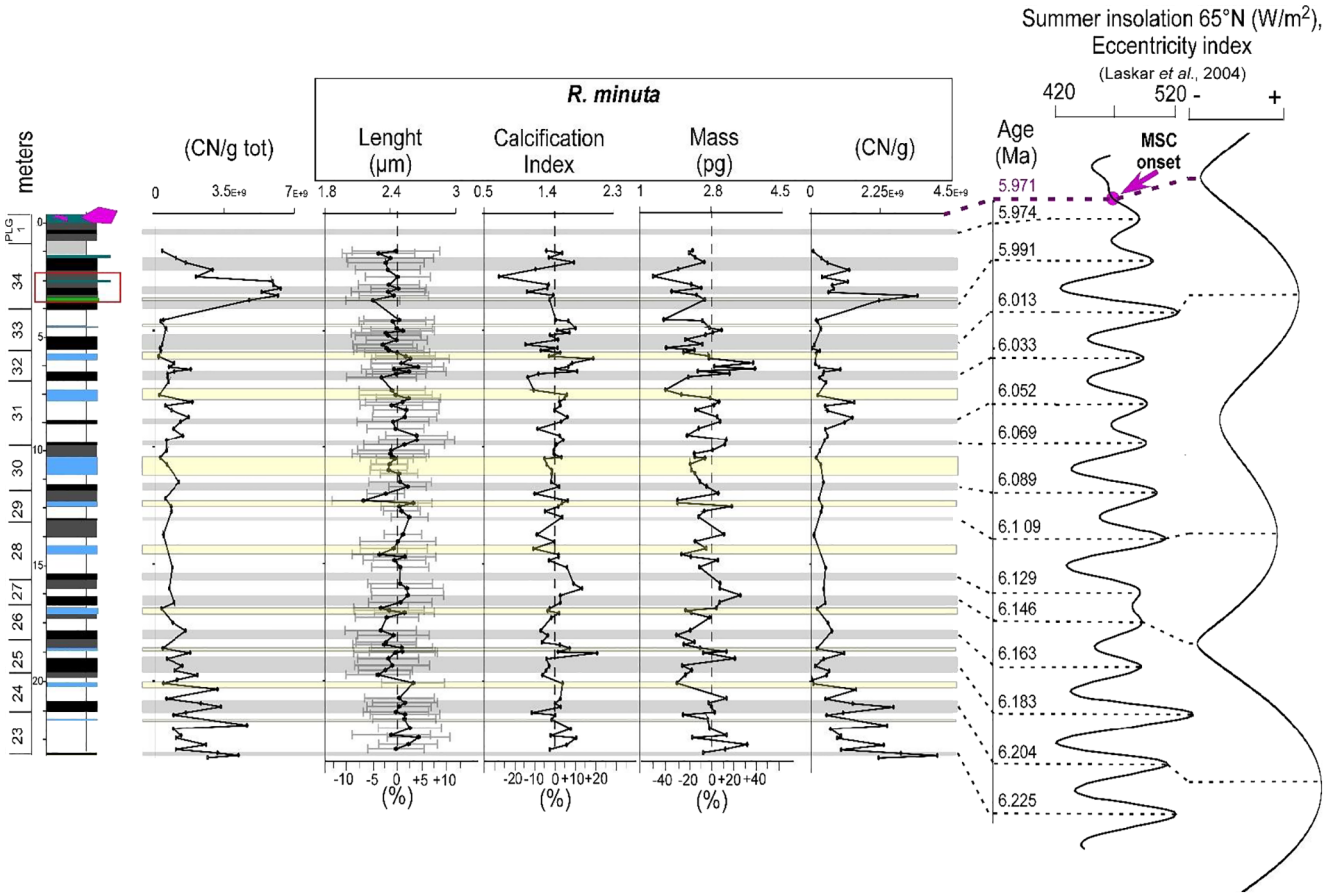


**Figure 8.** *Reticulofenestra minuta* biometric measurement and absolute abundance in the Perales section compared with the change in orbital parameters (precession and eccentricity from Laskar et al. [2004]). The error bars represent the standard deviation. The dashed line represents the mean average, the lower axis shows the variation expressed in % from the mean average. The red rectangle indicates the position of the Messinian Salinity Crisis onset bioevent (Mancini et al., 2020). Legend as in Figure 4.

### 3.5. *Reticulofenestra minuta*

*Reticulofenestra minuta* is the main contributor to the total coccolith concentration in the Perales section as revealed by the calcareous nannofossil absolute abundance (Figure 8). High absolute abundance of this taxon is recorded preferentially in the lower part of the studied section (UA23 and UA24) and in the last pre-evaporitic cycle (UA34), where *R. minuta* exceed the $1.5 \times 10^9$ CN/g.

The average length of the *R. minuta* spans from 2.1 to 2.6 µm, with the lowest size and mass values recorded generally in the diatomite and the highest in the sapropel layers. The *R. minuta* length and mass are positively correlated ($R^2 = 0.6417$, Figure 3b) and show a similar trend (Figure 8). Differently, *R. minuta* calcification index is not correlated with the length and mass ($R^2 = 0.0265$ and $R^2 = 0.0276$, Figure S4). *Reticulofenestra minuta* mass shows a decreasing trend from UA32 toward the MSC onset, with lowest value in the cycle UA34 where a statistically significant size decrease was recorded (Figures 7 and S2).

## 4. Discussion

### 4.1. Size Decrease During MSC Onset Bioevent and Productivity Change

As revealed by the ANOVA and Tukey HSD test (Figures S2 and S3) a statistically relevant size decrease affected *H. carteri*, *S. abies*, and *U. rotula* (*U. rotula* was tested in the Perales sections only), concomitant with an increase in CN absolute abundance recorded in the cycle UA34 (Figures 4, 6, and 7). Calcareous nannofossils absolute abundance in the sedimentary record is extensively used to track changes in CN

productivity through the geological past (Browning & Watkins, 2008; Flores et al., 1997; Gibbs et al., 2018; López-Otálvaro et al., 2008). We excluded that the recorded increase in CN absolute abundance was due to a concentration factor as a results of a slowdown of the sedimentation rate, because the precessional cycle bearing the MSC onset bioevent in the Perales section is roughly twice as thick as compared with the other UA cycles. It can be inferred that the increased CN absolute abundance concomitant with a size reduction is not related to the slowdown of the sedimentation rate but represents a primary signal, thus indicating an increase in the calcareous nannoplankton productivity.

In our study, the recorded size reduction took place during a very peculiar event characterized by a distinct fossil signal approximating the MSC onset in several Mediterranean successions (Faneromeni, Pissouri, Polemi Basin, Tokhni, Falconara, Fanantello, Lemme, Pollenzo, Banengo, Moncalvo, and Sorbas; Gennari et al., 2018; Lozar & Negri, 2019; Lozar et al., 2018; Mancini et al., 2020). This event was first identified by Lozar et al. (2018) and described as a succession of CN peak in abundance of the species *S. abies*, *H. carteri*, *U. rotula*, and *R. clavigera*. This event was recently referred as MSC onset bioevent (Mancini et al., 2020), and marks the last restriction pulse affecting the Mediterranean Basin and triggering the MSC onset (Mancini et al., 2020). The decreased water exchange between the Mediterranean Sea and the Atlantic Ocean increased the sensitivity of the Mediterranean Sea to continental runoff and associated nutrient supply into the basin, ultimately resulting in enhanced marine productivity (Mancini et al., 2020). A further outcome of this study is the possibility to use the CN size reduction as a biostratigraphic signal in those sections in which it is masked by the cyclical peaks of the species involved in the MSC onset bioevent (e.g., Tokhni section, Gennari et al., 2018; Perales section, Mancini et al., 2020). However, several samples encompassing several precessional cycle needed to be analyzed in order to discern the size variation during the MSC onset bioevent, since the recorded absolute values of the CN sizes is not comparable between the 3 sections studied.

High CN absolute abundances are also recorded in the cycles UA23 and UA24 ($4.64 \times 10^9$ CN/g and $3.54 \times 10^9$ CN/g, respectively (Figure 8)), but not associated with noticeable size decreases. This suggests either that the CN growth rate alone was likely not high enough for driving any relevant size change, or the mechanisms leading to size reduction are likely associated with the triggering factors inducing the enhanced CN productivity. Therefore, we hypothesized that the CN size decrease concomitant with high CN abundance recorded during the MSC onset bioevent could be linked to the enhanced freshwater influence delivering nutrients and the associated changes in the water column structure (Mancini et al., 2020). Differently, in the lower UA23 and UA24 cycles, indication of important freshwater input was not recorded and the CN high abundance encountered in these cycles could be explained as a result of a diminished sedimentation rate resulting in highest concentration of CN in the bulk sediment. From this observation, it could be inferred that the enhanced freshwater input and the associated changes in the water column structure, turbidity and nutrients delivery are the primary candidates for explain the CN size reduction accompanying the MSC onset. Since the increase in water turbidity cannot explain high CN absolute abundance, we infer that the nutrient delivery may have had the primary control on the CN size reduction. In the Eastern Mediterranean, Karakitsios et al. (2017) show a sharp freshwater input occurring between 6.45 and 6.121 Ma evidenced by *H. carteri*, *C. leptoporus*, *U. jafari*, *R. haqii*, and *Reticulofenestra minutula*; this event was probably local since no evidence of such freshening has been detected further West in the Sorbas basin.

The relationship between the nutrient regime and coccolithophores size was highlighted by some culture experiments, in which the taxa *C. leptoporus*, *C. quadriperforatus*, *H. carteri*, and *Emiliania huxleyi* show that during the exponential growth phase, characterized by a rapid cell division rate, small cells (characterized by a low number of interlocking coccoliths) are produced (Gibbs et al., 2006, 2013; Sheward et al., 2017; Šupraha et al., 2015). Conversely, larger cells (with higher number of coccoliths) are produced during slow cell division (Gibbs et al., 2013; Sheward et al., 2017). Taking into account that a correlation could exist between the coccosphere size, the number of coccoliths covering the cell and the coccoliths size (Aloisi, 2015; Gibbs et al., 2013; Henderiks & Rickaby, 2007), an assessment of the cell division rate can be inferred from morphometrical changes measured on the coccoliths, as already performed by Gibbs et al. (2013, 2018) in the sediments straddling the Paleocene-Eocene thermal maximum (PETM). The size reduction affecting *H. carteri*, *S. abies*, and *U. rotula*, and the highest CN productivity recorded, could be the results of rapid cell division, occurred during period of excess nutrient availability and favorable water column structure (e.g.,

it was reconstructed that S. *abies* exploited nutrients in the deep photic zone when thermal stratification occurred, Flores et al., 2005; Mancini et al., 2020). In our study, similar morphometric changes were not observed in *C. pelagicus*, which is in line with the culture experiments that showed no significant coccolith size change related to experimental conditions (i.e., stationary growth phase vs. exponential growth phase; Gibbs et al., 2013; Sheward et al., 2017). However, draw a parallel between the fossil record and the laboratory experiments could be rather speculative, since some taxa considered in our study are extinct and the coccolithophores response to the environmental variables could be strain-specific, as demonstrated for *C. pelagicus* (Gibbs et al., 2013; Henderiks & Rickaby, 2007; Sheward et al., 2017). Differently from other coccolithophore taxa, *C. pelagicus* morphology was not affected also during the PETM, likely because of its insensitivity to the broad $pCO_2$ variation that characterized this event (Henderiks & Rickaby, 2007).

Therefore, we infer that during the MSC CN bioevent, *S. abies*, *H. carteri*, and *U. rotula* shifted to more r-selected strategy, by increasing their cell division rate to exploit nutrients during seasonal favorable conditions. This resulted in a size decrease and in an increase in CN absolute abundance (Figure 8).

In other geological case histories, the CN size reduction is often reported to be related to "stressed" conditions (Faucher, Erba, et al., 2017) and the CN size increase with stable conditions (Ferreira et al., 2017). However, our results show that the CN size reduction occurred during period characterized by high CN productivity, thus indicating optimal environmental condition for calcareous nannoplankton to growth rather than stressed environment, at least during the MSC onset bioevent. Relevant size decreases were recorded during Oceanic Anoxic Events (Erba et al., 2010; Faucher, Erba, et al., 2017; Lübke & Mutterlose, 2016) in relation with abrupt increase in $CO_2$ emissions (and the consequent pH decrease in surface water) (Erba et al., 2010), toxic metal increase (Faucher, Hoffmann, et al., 2017), or with an increase in continental runoff and the associated increase in water turbidity (Lübke & Mutterlose, 2016). Generally, the amplitude of the CN size reduction during the OAEs is comparable to that recorded during the MSC CN bioevent (Erba et al., 2019).

After the MSC onset, the CN productivity gradually decreased and the CN size (*H. carteri*, *S. abies*, and *U. rotula*) oscillates without reaching the previous size average. The basin restriction occurring during the MSC CN bioevent amplified the sensitivity of the Mediterranean Basin to external forces, such as temperature change, freshwater input, and nutrient delivery (Mancini et al., 2020). This ultimately may resulted in an increased environmental variability, which could fall within the definition of "stressed" conditions. An attempt of comparison between the paleoenvironment straddling the MSC with actual analog could be provided by modern lagoon environments (e.g., in the Términos Lagoon, SE Gulf of Mexico), in which strong changes in salinity, productivity and turbidity occurred in response mainly to seasonal change in the freshwater input (Poot-Delgado et al., 2015; Yáñez-Arancibia & Day, 2005). Coccolithophores were recorded in some lagoon environments (Poot-Delgado et al., 2015; Sakka et al., 1999) showing distribution pattern according mainly to seasonal variations (Poot-Delgado et al., 2015). Therefore, it could be inferred that after the MSC onset bioevent, calcareous nannoplankton were likely affected by strong environmental variability because of the increased basin restriction; they were forced to increase the cell division rate to face and survive the rapid development of hostile environmental conditions, such as rapid and extreme changes in salinity and nutrient delivery.

In our studied sections, the MSC onset bioevent is often accompanied by the disappearance of normal size planktic foraminifers (>125 μm; Lozar et al., 2018; Violanti et al., 2013); the assemblage is dominated by dwarf foraminifers in the 43–125 μm size fraction (Figure 9). The record of dwarf planktic foraminifers during the MSC interval was already reported in cores and land sections (Braga et al., 2006; Cita et al., 1978; Fortuin & Krijgsman, 2003; Hsü et al., 1978; Iaccarino & Bossio, 1999; Riding et al., 1998; van de Poel, 1992), and interpreted as the result of "stressed" or "anomalous" water column condition (Corbí et al., 2016), although some authors suggested that dwarf planktonic foraminifers were symptomatic of high nutrients input (Kaiho et al., 2006; van de Poel, 1992). We suggest that the anomalous or stressed conditions were likely related to the restriction of the Mediterranean Basin, that resulted in an increase in the environmental variability (e.g., increase in the freshwater input and the associated nutrients delivery) which forced also the foraminifers to faster complete their life cycle and hence, to reduce their size (Figure 9).

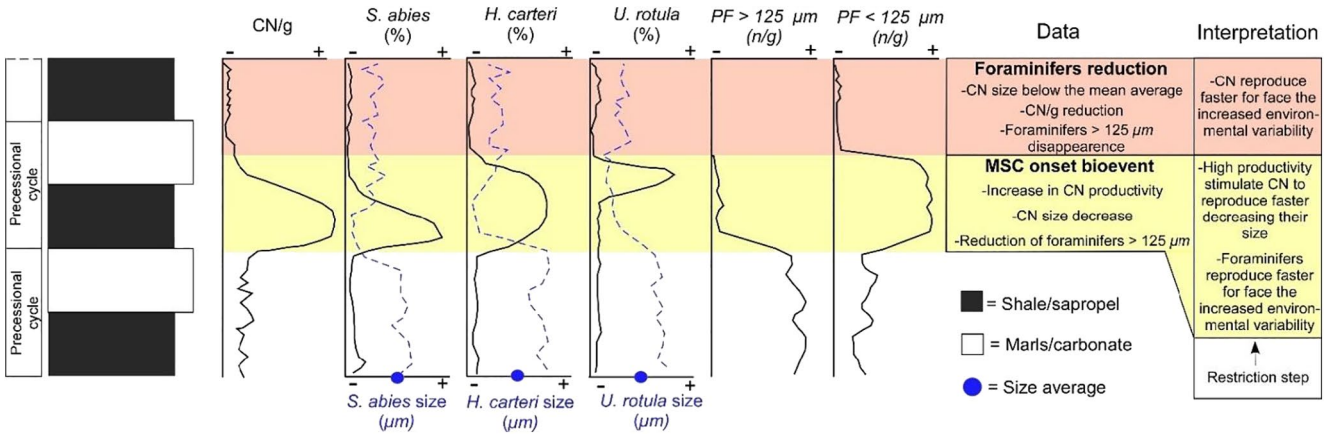


**Figure 9.** Schematic representation that summarize the calcareous nannofossils size and abundance and foraminifer size fraction fluctuations accompanying the Messinian Salinity Crisis onset bioevent in the three studied sections (see Section 4.1 for explanation).

### 4.2. *Reticulofenestra Minuta* Size as a Tracer for Precessional Variability

Very little is known about how orbital forcing affects climate and environmental change and how this is linked to coccolithophore size. Suchéras-Marx et al. (2010) highlight the relevance of orbital-controlled environmental factors influencing CN morphometric parameters. To test this hypothesis, our analysis was restricted to *R. minuta*, which dominated the assemblage throughout the studied interval in the Perales section.

Our results reveal a good correlation between *R. minuta* size and mass and the lithological changes of the sedimentary quadripartite cycle (Figure 3b), deposited under precessional control (Sierro et al., 2003). *Reticulofenestra minuta* shows minimum in the average length and mass during diatomite deposition (Figures 3b and 8). The diatomites were usually characterized by a mixture of CN and foraminifers with paleoecological affinity for either warm/oligotrophic, cold/eutrophic (i.e., warm-oligotrophic/cold-eutrophic index of Sierro et al. [2003]; i.e., *C. pelagicus*, Mancini et al., 2020), and/or salinity decrease (i.e., *H. carteri*, Mancini et al., 2020). Despite the diatoms-based information are available only for the lower cycle of the UA (i.e., UA5 – UA8; Pérez-Folgado et al., 2003), a strong seasonality is suggested to characterize these lithologies because of the presence of *Thalassionema* and *Rhizosolenia*. The former is generally associated with the cold season and enhanced surface primary productivity (McKenzie et al., 1979; Moissette & Saint Martin, 1992), while the latter is generally associated to the warm season and to a Deep Chlorophyll Maximum development (Kemp & Villareal, 2013; Margalef, 1978). Based on these evidence, it was inferred that the diatomite were deposited in an environment characterized by strong seasonality, with enhanced runoff inducing stratification during warm/humid phases and vigorous vertical mixing during cold/drier phases (Mancini et al., 2020).

On the opposite, *R. minuta* size and mass show higher value in the upper part of the sapropel partitioning (Figures 3b and 8), where the available proxies point to a stable and strongly stratified water column (Filippelli et al., 2003; Flores et al., 2005; Mancini et al., 2020; Pérez-Folgado et al., 2003; Reghizzi et al., 2017; Sierro et al., 2003).

From cycle UA31 toward the MSC onset, the mass of *R. minuta* shows higher fluctuation amplitude with the tendency toward lower values (Figure 8), likely reflecting an increase in the environmental variability at the precessional scale, that could be attributed to the climate sensitivity amplification induced by the restriction step occurred at ~6.03 Ma and recorded in the nearby Bajo Segura Basin (Corbí et al., 2020) and in the whole Mediterranean approximately at the same time (Gennari et al., 2018; Kouwenhoven et al., 2006). The same response was recorded in the foraminiferal diversity index and in the benthic foraminiferal absolute abundance in the Perales section (Sierro et al., 2003), marking an increase in the environmental instability toward the MSC onset. In this framework, it is reasonable inferring that the drivers of the *R. minuta* size decrease are related to unstable environmental condition that occurred within an annual cycle, leading *R.*

*minuta* to reproduce faster to face the unstable environmental condition during the diatomite deposition and toward the MSC onset.

### 4.3. The Possible Role of $pCO_2$ on Calcareous Nannoplankton Size

In recent years, many studies focused on the calcareous nannoplankton response to the ongoing ocean acidification and warming (Iglesias-Rodriguez et al., 2008; Langer et al., 2006, 2009; Meyer & Riebesell, 2015; Zondervan, 2007), caused by substantial accumulation of anthropogenic $CO_2$ emissions in the atmosphere, and the consequent impact on the biological carbon pump (Rost & Riebesell, 2004; Ziveri et al., 2007). The geological record offers many opportunities to study rapid environmental perturbations and their impact on the biota. For instances the Paleocene-Eocene Thermal Maximum (PETM) is often compared to the current anthropogenic climate change, although the rate of $CO_2$ emission is several times lower compared to the present scenarios (Zeebe et al., 2016).

The late Miocene was characterized by a rapid decline in the global sea surface temperature (6°C between 30° and 60°N within 7.5–5.5 Ma; Herbert et al., 2016), likely related to the decrease in $pCO_2$ inferred from the stable isotopes of coccolithophores and changes in the global vegetation covering (Bolton & Stoll, 2013; Bolton et al., 2016; Herbert et al., 2016). Recent studies underline the relevance of the MSC on the decline in $CO_2$ content occurring during the late Miocene, as the result of limited water exchange between the Mediterranean Sea and the Atlantic Ocean (Capella et al., 2019). Interestingly, we noted that the late Miocene cooling trend (Herbert et al., 2016) fits with the Coccolithophore Assemblage Size (CAS, Herrmann & Theirstein, 2012) and with the onset of the MSC (Figure 10). Henderiks and Pagani (2008) speculate that the shift toward smaller size of the reticulofenestrids during the Oligocene reflects an adaptive response to a decrease in $pCO_2$. However, this physiological adaptation to $pCO_2$ fluctuations is species specific and for instance did not affected *C. pelagicus* (Gibbs et al., 2013; Henderiks & Rickaby, 2007). The size reduction affecting some selected species during the MSC CN bioevent occurred abruptly, does not fit the gradual decrease in temperature (and $pCO_2$) inferred from late Miocene records (Herbert et al., 2016). Moreover the calculated sea surface temperature in the East Mediterranean during the Messinian (from 6.45 to 5.97 Ma) did not reveals any cooling trend toward the MSC onset (Vasiliev et al., 2019). Consequently, the size reduction during the MSC onset bioevent was likely not directly related to the ongoing global decrease in temperature and $pCO_2$. Differently, the cyclical *R. minuta* size and mass fluctuation could be related with precession-induced $pCO_2$ variability, but this inference remains speculative, because of the scarcity of knowledge regarding the $pCO_2$ trend and its variability at the precessional scale throughout the late Miocene.

Although the trigger for the CN size reduction during MSC CN bioevent was likely related to local environmental changes, further efforts are necessary to better understand the sparse but striking data regarding the correlation within CN size, $pCO_2$ and MSC onset.

## 5. Conclusion

Calcareous nannofossil biometry and absolute abundance analyses were performed in the Sorbas Basin (Perales section) and in the Piedmont Basin (Banengo and Pollenzo sections) in order to highlight the impact of the MSC onset on marine organisms and ultimately decipher the paleoenvironmental dynamics spanning this time interval.

An increase in the CN absolute abundance, concomitant with a size decrease of *H. carteri*, *S. abies*, and *U. rotula* was recorded at the time of the MSC onset bioevent. These morphometric changes are in the same order of magnitude of those reported during major environmental perturbations during Earth history. These size reductions were likely related to an increase in calcareous nannoplankton productivity that led to selected calcareous nannoplankton taxa to increase the overall growth rate and decreasing their size, as supported by laboratory culture experiments. Calcareous nannoplankton productivity was triggered by a restriction pulse affecting the Atlantic-Mediterranean gateway that increased the continental runoff and the associated nutrient delivery influence in the Mediterranean Sea approximately at the MSC onset. After the MSC onset bioevent, the analyzed taxa did not recover their normal size, and their mean size always fluctuated below the mean average, in parallel with a drastic reduction of CN absolute abundance. In this

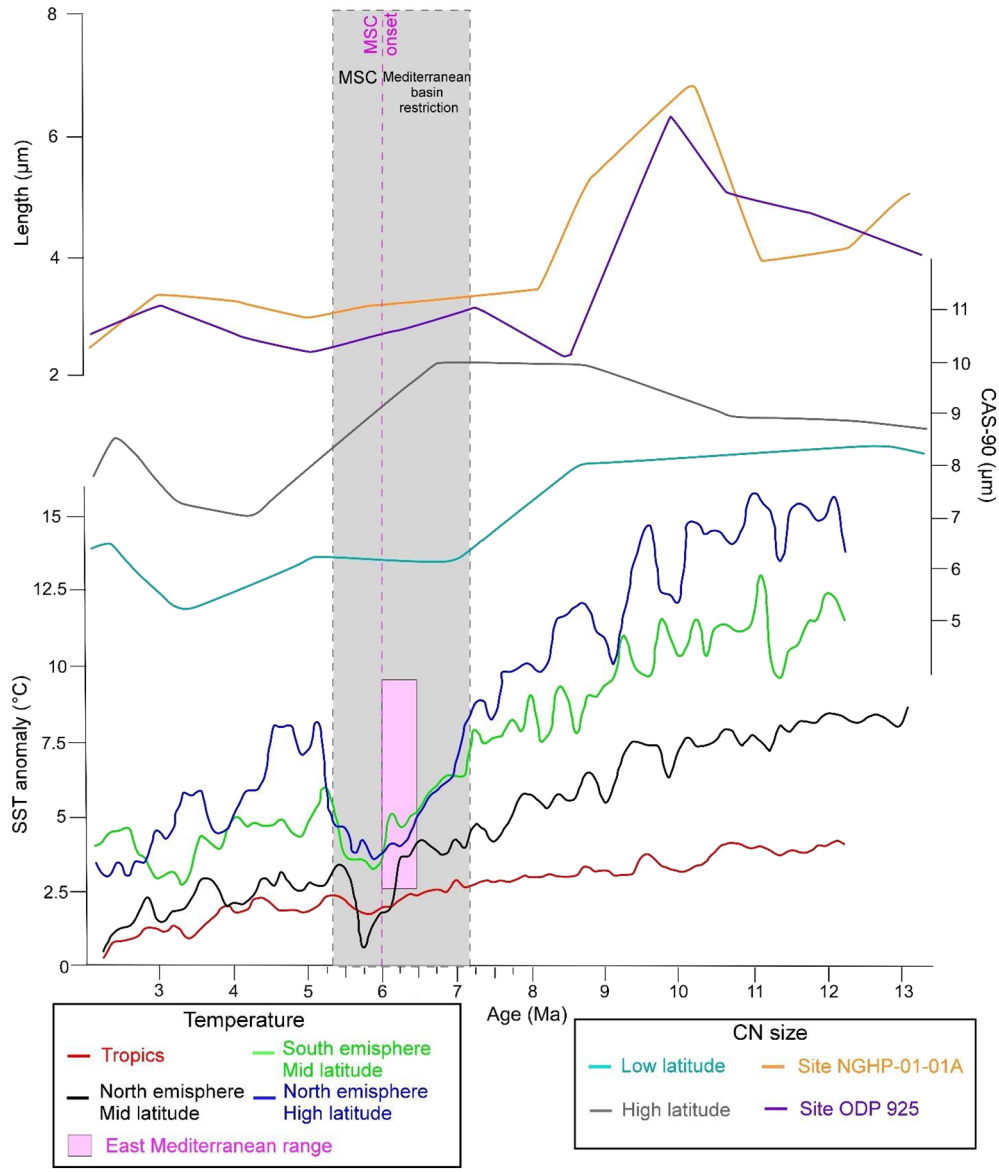


**Figure 10.** Sea surface temperature evolution based on alkenone record over the late Miocene and Pliocene (Herbert et al., 2016; Vasiliev et al., 2019) compared with the 90th percentile of Coccoliths Assemblage Size (CAS-90) (Herrmann & Thierstein, 2012) and the Noëlaerhabdaceae coccolith length (Bolton et al., 2016). The gray rectangle marks the period of the Mediterranean Basin restriction and of the Messinian Salinity Crisis (Capella et al., 2019). The blue line represents the temperature evolution at high latitudes (>50°N) in the North Hemisphere; the green line represents the temperature evolution at mid latitudes (30°–50°S) in the South Hemisphere; the black line represents the temperature evolution at mid latitudes (30°–50°N) in the North Hemisphere; the red line represents the temperature evolution at the tropics (Herbert et al., 2016). The violet rectangle represents the East Mediterranean sea surface temperature range (Vasiliev et al., 2019). The cyan and the gray lines represent the means of CAS-90 evolution at the low latitudes (<45°) and at high latitudes (>45°). The orange and the violet lines represent the Noëlaerhabdaceae coccolith length measured at the site NGHP 01-01A (Indian Ocean) and at the ODP site 925 (Atlantic Ocean), respectively. Data from Herbert et al. (2016), Herrmann and Thierstein (2012), and Bolton et al. (2016); redrawn after Herbert et al. (2016) and Bolton et al. (2016).

case, dwarf CN are symptomatic of a highly variable environment, comparable with actual lagoonal system in which the environmental parameters are strongly modulated by the freshwater input.

Our analysis also reveals that *R. minuta* size and mass cyclically fluctuate mimicking the precession curve, revealing that such size decrease occurs during time interval characterized by strong seasonal variability,

corresponding to the diatomite layer in the Perales section. The *R. minuta* size and mass fluctuation amplitude increases from ~6.03 toward the MSC onset, where it shows the lowest values. Also in this case, smaller CN were related to unstable water column conditions, which forced CN (and foraminifers, toward the MSC onset) to reproduce faster and decrease their size to face the unstable environmental conditions.

The influence of the gradual global decline of $pCO_2$, characterizing the Messinian, was not responsible for the size reduction recorded during the MSC onset bioevent, although a possible role governing the size variability of *R. minuta* at the precessional scale cannot completely be discarded.

## Conflict of Interest

The authors declare no conflicts of interest relevant to this study.

## Data Availability Statement

The generated data set is stored on Zenodo repository (https://zenodo.org/record/4569513#.YDz5k2hKg2w).

**Acknowledgments**
The authors thank to the three anonymous reviewers that improved the overall quality of the manuscript. Open Access Funding provided by Universita degli Studi di Torino within the CRUI-CARE Agreement.

## References

Aloisi, G. (2015). Covariation of metabolic rates and cell size in coccolithophores. *Biogeosciences*, *12*, 4665–4692. https://doi.org/10.5194/bg-12-4665-2015

Baggley, K. A. (2000). The late Tortonian-early Messinian foraminiferal record of the Abad Member (Turre formation), Sorbas Basin, Almería, south-east Spain. *Palaeontology*, *43*, 1069–1112. https://doi.org/10.1111/1475-4983.00162

Beaufort, L., Barbarin, N., & Gally, Y. (2014). Optical measurements to determine the thickness of calcite crystals and the mass of thin carbonate particles such as coccoliths. *Nature Protocols*, *9*, 633–642. https://doi.org/10.1038/nprot.2014.028

Beaufort, L., & Dollfus, D. (2004). Automatic recognition of coccoliths by dynamical neural networks. *Marine Micropaleontology*, *51*(1–2), 57–73. https://doi.org/10.1016/j.marmicro.2003.09.003

Beaufort, L., Probert, I., de Garidel-Thoron, T., Bendif, E. M., Ruiz-Pino, D., Metzl, N., et al. (2011). Sensitivity of coccolithophores to carbonate chemistry and ocean acidification. *Nature*, *476* (7358), 80–83. https://doi.org/10.1038/nature10295

Blanc, P.-L. (2006). Improved modelling of the Messinian Salinity Crisis and conceptual implication. *Palaeogeography, Palaeoclimatology, Palaeoecology*, *238*, 349–372. https://doi.org/10.1016/j.palaeo.2006.03.033

Bollmann, J., & Herrle, H. O. (2007). Morphological variation of *Emiliania huxleyi* and sea surface salinity. *Earth and Planetary Science Letters*, *255*(3–4), 273–288. https://doi.org/10.1016/j.epsl.2006.12.029

Bolton, C. T., Hernández-Sánchez, M. T., Fuertes, M. A., González-Lemos, S., Abrevaya, L., Mendez-Vicente, A., et al. (2016). Decrease in coccolithophore calcification and $CO_2$ since the middle Miocene. *Nature Communications*, *7*(1), 1–13. https://doi.org/10.1038/ncomms10284

Bolton, C. T., & Stoll, H. M. (2013). Late Miocene threshold response of marine algae to carbon dioxide limitation. *Nature*, *500*, 558–562. https://doi.org/10.1038/nature12448

Bourillot, R., Vennin, E., Rouchy, J. M., Durlet, C., Rommevaus, V., Kolodka, C., & Knap, F. (2009). Structure and evolution of a Messinian mixed carbonate-siliciclastic platform: The role of evaporites (Sorbas Basin, South-east Spain). *Sedimentology*, *57*, 477–512. https://doi.org/10.1111/j.1365-3091.2009.01092.x

Braga, J. C., Martin, J. M., Riding, R., Aguirre, J., Sanchez-Almazo, I. M., & Dinares-Turell, J. (2006). Testing models for the Messinian salinity crisis: The Messinian record in Almeria, SE Spain. *Sedimentary Geology*, *188–189*, 131–154. https://doi.org/10.1016/j.sedgeo.2006.03.002

Browning, E. L., & Watkins, D. K. (2008). Elevated primary productivity of calcareous nannoplankton associated with ocean anoxic event 1b during the Aptian/Albian transition (Early Cretaceous). *Paleoceanography*, *23*(2). https://doi.org/10.1029/2007pa001413

Capella, W., Flecker, R., Hernández-Molina, F. J., Simon, D., Meijer, P. T., Rogerson, M., et al. (2019). Mediterranean isolation preconditioning the Earth System for late Miocene climate cooling. *Scientific Reports*, *9*, 3795. https://doi.org/10.1038/s41598-019-40208-2

Cita, M. B., Wright, R. C., Ryan, W. B. F., & Longinelli, A. (1978). Messinian paleoenvironments. In K. J. Hsü, L. Montadert, D. Bernoulli, M. B. Cita, A. Erickson, R. E. Garrison, et al. (Eds.), *Initial Reports Deep Sea Drilling Project* (Vol. 42, pp. 1003–1035). https://doi.org/10.2973/dsdp.proc.42-1.153.1978

Clauzon, G., Suc, J. P., Do Couto, D., Jouannic, G., Melinte-Dobrinescu, M. C., Jolivet, L., et al. (2015). New insights on the Sorbas Basin (SE Spain): The onshore reference of the Messinian salinity crisis. *Marine and Petroleum Geology*, *66*, 71–100. https://doi.org/10.1016/j.marpetgeo.2015.02.016

Corbí, H., & Soria, J. M. (2016). Late Miocene–early Pliocene planktonic foraminifer event-stratigraphy of the Bajo Segura basin: A complete record of the western Mediterranean. *Marine and Petroleum Geology*, *77*, 1010–1027. https://doi.org/10.1016/j.marpetgeo.2016.08.004

Corbí, H., Soria, J. M., Giannetti, A., & Yébenes, A. (2020). The step-by-step restriction of the Mediterranean (start, amplification, and consolidation phases) preceding the Messinian Salinity Crisis (climax phase) in the Bajo Segura basin. *Geo-Marine Letters*, *40*, 1–361. https://doi.org/10.1007/s00367-020-00647-7

Corbí, H., Soria, J. M., Lancis, C., Giannetti, A., Tent-Manclús, J. E., & Dinares-Turell, J. (2016). Sedimentological and paleoenvironmental scenario before, during, and after the Messinian Salinity Crisis: The San Miguel de Salinas composite section (western Mediterranean). *Marine Geology*, *379*, 246–266. https://doi.org/10.1016/j.margeo.2016.05.017

D'Amario, B., Pérez, C., Grelaud, M., Pitta, P., Krasakopoulou, E., & Ziveri, P. (2020). Coccolithophore community response to ocean acidification and warming in the Eastern Mediterranean Sea: Results from a mesocosm experiment. *Scientific Reports*, *10*(1), 1–14. https://doi.org/10.1038/s41598-020-69519-5

D'Amario, B., Ziveri, P., Grelaud, M., & Oviedo, A. (2018). *Emiliania huxleyi* coccolith calcite mass modulation by morphological changes and ecology in the Mediterranean Sea. *PloS One*, *13*(7), e0201161. https://doi.org/10.1371/journal.pone.0201161

de Bodt, C., Oostende, N. V., Harlay, J., Sabbe, K., & Chou, L. (2010). Individual and interacting effects of $pCO_2$ and temperature on *Emiliania huxleyi* calcification: Study of the calcite production, the coccolith morphology and the coccosphere size. *Biogeosciences*, *7*(5), 1401–1412. https://doi.org/10.5194/bg-7-1401-2010

Dedert, M., Stoll, H., Kars, S., Young, J. R., Shimizu, N., Kroon, D., et al. (2014). Temporally variable diagenetic overgrowth on deep-sea nannofossil carbonates across Palaeogene hyperthermals and implications for isotopic analyses. *Marine Micropaleontology*, *107*, 18–31. https://doi.org/10.1016/j.marmicro.2013.12.004

Dela Pierre, F., Bernardi, E., Cavagna, S., Clari, P., Gennari, R., Irace, A., et al. (2011). The record of the Messinian salinity crisis in the Tertiary Piedmont Basin (NW Italy): The Alba section revisited. *Palaeogeography, Palaeoclimatology, Palaeoecology*, *310*, 238–255. https://doi.org/10.1016/j.palaeo.2011.07.017

Engel, A., Zondervan, I., Aerts, K., Beaufort, L., Benthien, A., Chou, L., et al. (2005). Testing the direct effect of $CO_2$ concentration on a bloom of the coccolithophorid *Emiliania huxleyi* in mesocosm experiments. *Limnology and Oceanography*, *50*(2), 493–507. https://doi.org/10.4319/lo.2005.50.2.0493

Erba, E., Bottini, C., Faucher, G., Gambacorta, G., & Visentin, S. (2019). The response of calcareous nannoplankton to Oceanic Anoxic Events: The Italian pelagic record. *Società Paleontologica Italiana*, *58*, 51–71. https://doi.org/10.1126/science.1199608

Erba, E., Bottini, C., Weissert, H. J., & Keller, C. E. (2010). Calcareous nannoplankton response to surface-water acidification around Oceanic Anoxic Event 1a. *Science*, *329*, 428–432. https://doi.org/10.1126/science.1188886

Faucher, G., Erba, E., Bottini, C., & Gambacorta, G. (2017). Calcareous nannoplankton response to the latest Cenomanian Oceanic Anoxic Event 2 perturbation. *Research in Paleontology and Stratigraphy*, *123*(1), 159–175. https://doi.org/10.1126/science.1199608

Faucher, G., Hoffmann, L. J., Bach, L. T., Bottini, C., Erba, E., & Riebesell, U. (2017). Impact of trace metal concentrations on coccolithophore growth and morphology: Laboratory simulations of Cretaceous stress. *Biogeosciences*, *14*, 3603–3613. https://doi.org/10.5194/bg-14-3603-2017

Faucher, G., Riebesell, U., & Bach, L. T. (2020). Can morphological features of coccolithophores serve as a reliable proxy to reconstruct environmental conditions of the past? *Climate of the Past*, *16*, 1007–1025. https://doi.org/10.5194/cp-16-1007-2020

Ferreira, J., Mattioli, E., & van de Schootbrugge, B. (2017). Palaeoenvironmental vs. evolutionary control on size variation of coccoliths across the Lower-Middle Jurassic. *Palaeogeography, Palaeoclimatology, Palaeoecology*, *465*, 177–192. https://doi.org/10.1016/j.palaeo.2016.10.029

Filippelli, G. M., Flores, J. A., Vázquez, R., Utrilla, R., Pérez-Folgado, M., Latimer, C., & Latimer, J. C. (2003). A sediment-nutrient-oxygen feedback responsible for productivity variations in late Miocene sapropel sequences of the western Mediterranean. *Palaeogeography, Palaeoclimatology, Palaeoecology*, *190*, 335–348. https://doi.org/10.1016/S0031-0182(02)00613-2

Flecker, R., Krijgsman, W., Capella, W., de Castro Martins, C., Dmitrieva, E., Mayser, J. P., et al. (2015). Evolution of the Late Miocene Mediterranean–Atlantic gateways and their impact on regional and global environmental change. *Earth-Science Reviews*, *150*, 365–392. https://doi.org/10.1016/j.earscirev.2015.08.007

Flores, J. A., Sierro, F. J., Filippelli, G. M., Barcena, M. A., Perez-Folgado, M., Vazquez, A., & Utrilla, R. (2005). Surface water dynamics and phytoplankton communities during deposition of cyclic late Messinian sapropel sequences in the western Mediterranean. *Marine Micropaleontology*, *56*, 50–79. https://doi.org/10.1016/j.marmicro.2005.04.002

Flores, J. A., Sierro, F. J., Francés, G., Vázquez, A., & Zamarren, I. (1997). The last 100,000 years in the western Mediterranean: Sea surface water and frontal dynamics as revealed by coccolithophores. *Marine Micropaleontology*, *29*(3-4), 351–366. https://doi.org/10.1016/S0377-8398(96)00029-1

Fortuin, A. R., & Krijgsman, W. (2003). The Messinian of the Nijar Basin (SE Spain): Sedimentation, depositional environments and paleogeographic evolution. *Sedimentary Geology*, *160*, 213–242. https://doi.org/10.1016/s0037-0738(02)00377-9

Gennari, R., Lozar, F., Turco, E., Dela Pierre, F., Manzi, V., Natalicchio, M., et al. (2018). Integrated stratigraphy and paleoceanographic evolution of the pre-evaporitic phase of the Messinian salinity crisis in the Eastern Mediterranean as recorded in the Tokhni section (Cyprus island). *Newsletter on Stratigraphy*, *51*, 33–55. https://doi.org/10.1127/nos/2017/0350

Gibbs, S. J., Bralower, T. J., Bown, P. R., Zachos, J. C., & Bybell, L. M. (2006). Shelf and open-ocean calcareous phytoplankton assemblages across the Paleocene-Eocene Thermal Maximum: Implications for global productivity gradients. *Geology*, *34*(4), 233–236. https://doi.org/10.1130/g22381.1

Gibbs, S. J., Poulton, A. J., Bown, P. R., Daniels, C. J., Hopkins, J., Young, J. R., et al. (2013). Species-specific growth response of coccolithophores to Palaeocene-Eocene environmental change. *Nature Geoscience*, *6*, 218–222. https://doi.org/10.1038/ngeo1719

Gibbs, S. J., Sheward, R. M., Bown, P. R., Poulton, A. J., & Alvarez, S. A. (2018). Warm plankton soup and red herrings: Calcareous nannoplankton cellular communities and the Palaeocene–Eocene Thermal Maximum. *Philosophical Transactions of the Royal Society A: Mathematical, Physical and Engineering Sciences*, *376*(2130), 20170075. https://doi.org/10.1098/rsta.2017.0075

Grelaud, M., Marino, G., Ziveri, P., & Rohling, E. J. (2012). Abrupt shoaling of the nutricline in response to massive freshwater flooding at the onset of the last interglacial sapropel event. *Paleoceanography*, *27*(3). https://doi.org/10.1029/2012pa002288

Hammer, Ø., Harper, D. A., & Ryan, P. D. (2001). PAST: Paleontological statistics software package for education and data analysis. *Palaeontologia Electronica*, *4*(1), 9. https://doi.org/10.1002/9780470750711

Henderiks, J., & Pagani, M. (2008). Coccolithophore cell size and the Paleogene decline in atmospheric $CO_2$. *Earth and Planetary Science Letters*, *269*, 576–584. https://doi.org/10.1016/j.epsl.2008.03.016

Henderiks, J., & Rickaby, R. E. M. (2007). A coccolithophore concept for constraining the Cenozoic carbon cycle. *Biogeosciences*, *4*, 323–329. https://doi.org/10.5194/bg-4-323-2007

Herbert, T. D., Lawrence, K. T., Tzanova, A., Peterson, L. C., Caballero-Gill, R., & Kelly, C. S. (2016). Late Miocene global cooling and the rise of modern ecosystems. *Nature Geoscience*, *9*, 843–847. https://doi.org/10.1038/ngeo2813

Herrmann, S., & Thierstein, H. R. (2012). Cenozoic coccolith size changes—Evolutionary and/or ecological controls? *Palaeogeography, Palaeoclimatology, Palaeoecology*, *333–334*, 92–106. https://doi.org/10.1016/j.palaeo.2012.03.011

Herrmann, S., Weller, A. F., Henderiks, J., & Thierstein, H. R. (2012). Global coccolith size variability in Holocene deep-sea sediments. *Marine Micropaleontology*, *82*(83), 1–12. https://doi.org/10.1016/j.marmicro.2011.09.006

Hsü, K. J., Montadert, L., Bernoulli, D., Cita, M. B., Erikson, A., Garrison, R. E., et al. (1978). Initial report of Deep Sea Drilling Project. *Mediterranean Sea* (Vol. 42). U.S. Government Printing Office. https://doi.org/10.2973/dsdp.proc.42-1.155.1978

Iaccarino, S. M., & Bossio, A. (1999). Paleoenvironment of uppermost Messinian sequences in the western Mediterranean (sites 974, 975 and 978). In R. Zahn, M. C. Comas, & A. Klaus (Eds.), *Proceedings of the Ocean Drilling Program. Scientific Results* (Vol. 161, pp. 529–540). Ocean Drilling Program. https://doi.org/10.2973/odp.proc.sr.161.246.1999

Iglesias-Rodriguez, M. D., Halloran, P. R., Rickaby, R. E. M., Hall, I. R., Colmenero-Hidalgo, E., Gittins, J. R., et al. (2008). Phytoplankton calcification in a high-$CO_2$ world. *Science*, *320*, 336–340. https://doi.org/10.1126/science.1154122

Kaiho, K., Takeda, K., Petrizzo, M. R., & Zachos, J. C. (2006). Anomalous shifts in tropical Pacific planktonic and benthic foraminiferal test size during the Paleocene–Eocene thermal maximum. *Palaeogeography, Palaeoclimatology, Palaeoecology*, *237*(2–4), 456–464. https://doi.org/10.1016/j.palaeo.2005.12.017

Karakitsios, V., Roveri, M., Lugli, S., Manzi, V., Gennari, G., Antonarakou, A., et al. (2017). A record of the Messinian salinity crisis in the eastern Ionian tectonically active domain (Greece, eastern Mediterranean). *Basin Research*, *29*, 203–233. https://doi.org/10.1111/bre.12173

Keller, G., & Abramovich, S. (2009). Lilliput effect in late Maastrichtian planktic foraminifera: Response to environmental stress. *Palaeogeography, Palaeoclimatology, Palaeoecology*, *284*, 47–62. https://doi.org/10.1016/j.palaeo.2009.08.029

Kemp, A. E. S., & Villareal, T. A. (2013). High diatom production and export in stratified waters–A potential negative feedback to global warming. *Progress in Oceanography*, *119*, 4–23. https://doi.org/10.1016/j.pocean.2013.06.004

Kouwenhoven, T. J., Morigi, C., Negri, A., Giunta, S., Krijgsman, W., & Rouchy, J. M. (2006). Palaeoenvironmental evolution of the eastern Mediterranean during the Messinian: Constraints from integrated microfossil data of the Pissouri Basin (Cyprus). *Marine Micropaleontology*, *60*, 17–44. https://doi.org/10.1016/j.marmicro.2006.02.005

Langer, G., Geisen, M., Baumann, K. H., Kläs, J., Riebesell, U., Thoms, S., & Young, J. R. (2006). Species-specific responses of calcifying algae to changing seawater carbonate chemistry. *Geochemistry, Geophysics, Geosystems*, *7*(9). https://doi.org/10.1029/2005gc001227

Langer, G., Nehrke, G., Probert, I., Ly, J., & Ziveri, P. (2009). Strain-specific responses of *Emiliania huxleyi* to changing seawater carbonate chemistry. *Biogeosciences*, *6*(11), 2637–2646. https://doi.org/10.5194/bg-6-2637-2009

Langer, G., Probert, I., Nehrke, G., & Ziveri, P. (2011). The morphological response of *Emiliania huxleyi* to seawater carbonate chemistry changes: An inter-strain comparison. *Journal of Nannoplankton Research*, *32*(1), 29–34. https://doi.org/10.5194/bg-6-2637-2009

Laskar, J., Robutel, P., Joutel, F., Gastineau, M., Correia, A. C. M., & Levrard, B. (2004). A long-term numerical solution for the insolation quantities of the Earth. *Astronomy & Astrophysics*, *428*(1), 261–285. https://doi.org/10.1051/0004-6361:20041335

López-Otálvaro, G. E., Flores, J. A., Sierro, F. J., & Cacho, I. (2008). Variations in coccolithophorid production in the Eastern Equatorial Pacific at ODP Site 1240 over the last seven glacial–interglacial cycles. *Marine Micropaleontology*, *69*(1), 52–69. https://doi.org/10.1016/j.marmicro.2007.11.009

Lozar, F., & Negri, A. (2019). A review of basin-wide calcareous nannofossil bioevents in the Mediterranean at the onset of the Messinian salinity crisis. *Marine Micropaleontology*, *151*, 101752. https://doi.org/10.1016/j.marmicro.2019.101752

Lozar, F., Violanti, D., Bernardi, E., Dela Pierre, F., & Natalicchio, M. (2018). Identifying the onset of the Messinian salinity crisis: A reassessment of the biochronostratigraphic tools (Piedmont Basin, NW Italy). *Newsletter on Stratigraphy*, *51/1*, 11–31. https://doi.org/10.1127/nos/2017/0354

Lübke, N., & Mutterlose, J. (2016). The impact of OAE 1a on marine biota deciphered by size variations of coccoliths. *Cretaceous Research*, *61*, 169–179. https://doi.org/10.1016/j.cretres.2016.01.006

Lübke, N., Mutterlose, J., & Bottini, C. (2015). Size variations of coccoliths in Cretaceous oceans—A result of preservation, genetics and ecology? *Marine Micropaleontology*, *117*, 25–39. https://doi.org/10.1016/j.marmicro.2015.03.002

Lugli, S., Manzi, V., Roveri, M., & Schreiber, B. C. (2010). The Primary Lower Gypsum in the Mediterranean: A new facies interpretation for the first stage of the Messinian salinity crisis. *Palaeogeography, Palaeoclimatology, Palaeoecology*, *297*, 83–99. https://doi.org/10.1016/j.palaeo.2010.07.017

Mancini, A. M., Gennari, R., Ziveri, P., Mortyn, P. G., Stolwijk, D. J., & Lozar, F. (2020). Calcareous nannofossil and foraminiferal trace element records in the Sorbas Basin: A new piece of the Messinian Salinity Crisis onset puzzle. *Palaeogeography, Palaeoclimatology, Palaeoecology*, *554*, 109796. https://doi.org/10.1016/j.palaeo.2020.109796

Manzi, V., Gennari, R., Hilgen, F., Krijgsman, W., Lugli, S., Roveri, M., & Sierro, F. J. (2013). Age refinement of the Messinian salinity crisis onset in the Mediterranean. *Terra Nova*, *25*, 315–322. https://doi.org/10.1111/ter.12038

Margalef, R. (1978). Life-forms of phytoplankton as survival alternatives in an unstable environment. *Oceanologica Acta*, *1*, 493–509.

MartÍn, J. M., Braga, J. C., Aguirre, J., & Betzler, C. (2004). Contrasting models of temperate carbonate sedimentation in a small Mediterranean embayment: The Pliocene Carboneras Basin, SE Spain. *Journal of the Geological Society*, *161*(3), 387–399. https://doi.org/10.1144/0016-764903-044

Mattioli, E., Pittet, B., Petitpierre, L., & Mailliot, S. (2009). Dramatic decrease of pelagic carbonate production by nannoplankton across the Early Toarcian anoxic event (T-OAE). *Global and Planetary Change*, *65*, 134–145. https://doi.org/10.1016/j.gloplacha.2008.10.018

Mattioli, E., Pittet, B., Young, J. R., & Bown, P. R. (2004). Biometric analysis of Pliensbachian-Toarcian (Lower Jurassic) coccoliths of the family Biscutaceae: Intra-and interspecific variability versus palaeoenvironmental influence. *Marine Micropaleontology*, *52*(1–4), 5–27. https://doi.org/10.1016/j.marmicro.2004.04.004

McKenzie, J. A., Jenkyns, H. C., & Bennet, G. G. (1979). Stable isotope study of the cyclic diatomite—Claystones from the Tripoli formation, Sicily: A prelude to the Messenian salinity crisis. *Palaeogeography, Palaeoclimatology, Palaeoecology*, *29*, 125–141. https://doi.org/10.1016/0031-0182(79)90077-4

Meier, K. J. S., Beaufort, L., Heussner, S., & Ziveri, P. (2014). The role of ocean acidification in *Emiliania huxleyi* coccolith thinning in the Mediterranean Sea. *Biogeosciences*, *11*, 2857–2869. https://doi.org/10.5194/bg-11-2857-2014

Meyer, J., & Riebesell, U. (2015). Responses of coccolithophores to ocean acidification: A meta-analysis. *Biogeosciences*, *12*, 1671–1682. https://doi.org/10.5194/bg-12-1671-2015

Milner, S., Langer, G., Grelaud, M., & Ziveri, P. (2016). Ocean warming modulates the effects of acidification on *Emiliania huxleyi* calcification and sinking. *Limnology and Oceanography*, *61*, 1322–1336. https://doi.org/10.1002/lno.10292

Modestou, S., Simon, D., Gutjahr, M., Marzocchi, A., Kowenhoven, T. J., Ellam, R. M., Flecker, R. (2017). Precessional variability of $^{87}Sr/^{86}Sr$ in the late Miocene Sorbas Basin: An interdisciplinary study of drivers of interbasin exchange. *Paleoceanography*, *32*, 1–22. https://doi.org/10.1002/2016PA003061

Moissette, P., & Saint Martin, J. P. (1992). Upwelling and benthic communities in the Messinian of western Mediterranean. *Paleontologia i Evolució*, *24*(25), 245–254.

Natalicchio, M., Dela Pierre, F., Birgel, D., Brumsack, H., Carnevale, G., Gennari, R., et al. (2019). Paleoenvironmental change in a precession-paced succession across the onset of the Messinian salinity crisis: Insight from element geochemistry and molecular fossils. *Palaeogeography, Palaeoclimatology, Palaeoecology*, *518*, 45–61. https://doi.org/10.1016/j.palaeo.2019.01.009

Negri, A., Capodonti, L., & Keller, J. (1999). Calcareous nannofossils, planktic foraminifers and oxygen isotope in the late Quaternary sapropels of the Ionian Sea. *Marine Geology*, *151*, 84–103. https://doi.org/10.1016/s0025-3227(98)00135-2

Oviedo, A., Ziveri, P., Alvarez, M., & Tanhua, T. (2015). Is coccolithophore distribution in the Mediterranean Sea related to seawater carbonate chemistry? *Ocean Science*, *11*, 13–32. https://doi.org/10.5194/os-11-13-2015

Paasche, E. (2002). A review of the coccolithophorid *Emiliania huxleyi* (Prymnesiophyceae), with particular reference to growth, coccolith formation, and calcification-photosynthesis interactions. *Phycologia*, *40*(6), 503–529. https://doi.org/10.2216/i0031-8884-40-6-503.1

Pérez-Folgado, M., Sierro, F. J., Bàrcena, M. A., Flores, J. A., Vàzquez, A., Utrilla, R., et al. (2003). Western versus eastern Mediterranean paleoceanographic response to astronomical forcing: A high-resolution microplankton study of precession-controlled sedimentary cycles during the Messinian. *Palaeogeography, Palaeoclimatology, Palaeoecology*, *190*, 317–334. https://doi.org/10.1016/S0031-0182(02)00612-0

Poot-Delgado, C. A., Okolodkov, Y. B., Aké-Castillo, J. A., & Rendón-von Osten, J. (2015). Annual cycle of phytoplankton with emphasis on potentially harmful species in oyster beds of Términos Lagoon, southeastern Gulf of Mexico. *Revista de Biología Marina y Oceanografía*, *50*, 465–477. https://doi.org/10.4067/s0718-19572015000400006

Reghizzi, M., Gennari, R., Douville, E., Lugli, S., Manzi, V., Montagna, P., et al. (2017). Isotope stratigraphy ($^{87}Sr/^{86}Sr$, $\delta^{18}O$, $\delta^{13}C$) of the Sorbas basin (Betic Cordillera, Spain): Paleoceanographic evolution across the onset of the Messinian salinity crisis. *Palaeogeography, Palaeoclimatology, Palaeoecology*, *469*, 60–73. https://doi.org/10.1016/j.palaeo.2016.12.039

Riding, R., Braga, J. C., Martin, J. M., & Sanchez-Almazo, I. M. (1998). Mediterranean Messinian salinity crisis: Constraints from a coeval marginal basin, Sorbas, southeastern Spain. *Marine Geology*, *146*, 1–20. https://doi.org/10.1016/s0025-3227(97)00136-9

Riebesell, U., Bach, L. T., Richard, G. J., Bellerby, R. G. J., Bermúdez Monsalve, R. J., Boxhammer, T., et al. (2016). Competitive fitness of a predominant pelagic calcifier impaired by ocean acidification. *Nature Geoscience*, *1*(1), 19–23. https://doi.org/10.1038/ngeo2854

Riebesell, U., Zondervan, I., Rost, B., Tortell, P. D., Zeebe, R. E., & Morel, F. M. M. (2000). Reduced calcification of marine plankton in response to increased atmospheric $CO_2$. *Nature*, *407*, 2–367. https://doi.org/10.1038/35030078

Rost, B., & Riebesell, U. (2004). Coccolithophores and the biological pump: Responses to environmental changes. In H. R. Thierstein & J. R. Young (Eds.), *Coccolithophores: From molecular processes to global impact* (pp. 99–125). Springer. https://doi.org/10.1007/978-3-662-06278-4_5

Sabino, M., Schefuß, E., Natalicchio, M., Dela Pierre, F., Birgel, D., Bortels, D., et al. (2020). Climatic and hydrologic variability in the northern Mediterranean across the onset of the Messinian salinity crisis. *Palaeogeography, Palaeoclimatology, Palaeoecology*, *545*, 109632. https://doi.org/10.1016/j.palaeo.2020.109632

Sakka, A., Legendre, L., Gosselin, M., LeBlanc, B., Delesalle, B., & Price, N. M. (1999). Nitrate, phosphate, and iron limitation of the phytoplankton assemblage in the lagoon of Takapoto Atoll (Tuamotu Archipelago, French Polynesia). *Aquatic Microbial Ecology*, *19*(2), 149–161. https://doi.org/10.3354/ame019149

Salaviale, C., Gollain, B., & Mattioli, E. (2018). Calcareous nannofossil fluxes and size fluctuations in the middle Eocene (48–39 Ma) from Ocean Drilling Program (ODP) Site 1209 in the tropical Pacific Ocean. *Palaeogeography, Palaeoclimatology, Palaeoecology*, *490*, 240–251. https://doi.org/10.1016/j.palaeo.2017.11.003

Salter, I., Schiebel, R., Ziveri, P., Movellan, A., Lampitt, R., & Wolff, G. A. (2014). Carbonate counter pump stimulated by natural iron fertilization in the Polar Frontal Zone. *Nature Geoscience*, *7*(12), 885–889. https://doi.org/10.1038/ngeo2285

Sheward, R. M., Poulton, A. J., Gibbs, S. J., Daniels, C. J., & Bown, P. R. (2017). Physiology regulates the relationship between coccosphere geometry and growth phase in coccolithophores. *Biogeosciences*, *14*, 1493–1509. https://doi.org/10.5194/bg-14-1493-2017

Sierro, F. J., Flores, J. A., Barcena, M. A., Vazquez, A., Utrilla, R., Zamarreno, I., et al. (2003). Orbitally-controlled oscillations in the planktic communities and cyclical changes in western Mediterranean hydrography during the Messinian. *Palaeogeography, Palaeoclimatology, Palaeoecology*, *190*, 289–316. https://doi.org/10.1016/s0031-0182(02)00611-9

Sierro, F. J., Hilgen, F. J., Krijgsman, W., & Flores, J. A. (2001). The Abad composite (SE Spain): A Mediterranean and global reference section for the Messinian. *Palaeogeography, Palaeoclimatology, Palaeoecology*, *168*, 141–169. https://doi.org/10.1016/S0031-0182(00)00253-4

Stoll, H. M., Guitian, J., Hernandez-Almeida, I., Mejia, L. M., Phelps, S., Polissar, P., et al. (2019). Upregulation of phytoplankton carbon concentrating mechanisms during low $CO_2$ glacial periods and implications for the phytoplankton $pCO_2$ proxy. *Quaternary Science Reviews*, *208*, 1–20. https://doi.org/10.1016/j.quascirev.2019.01.012

Suchéras-Marx, B., Mattioli, E., Pittet, B., Escarguel, G., & Suan, G. (2010). Astronomically-paced coccolith size variations during the early Pliensbachian (Early Jurassic). *Palaeogeography, Palaeoclimatology, Palaeoecology*, *295*, 281–292. https://doi.org/10.1016/j.quascirev.2019.01.01210.1016/j.palaeo.2010.06.006

Šupraha, L., Gerecht, A. C., Probert, I., & Henderiks, J. (2015). Eco-physiological adaptation shapes the response of calcifying algae to nutrient limitation. *Scientific Reports*, *5*(1), 1–8. https://doi.org/10.1038/srep16499

Tremolada, F., De Bernardi, B., & Erba, E. (2008). Size variations of the calcareous nannofossil taxon Discoaster multiradiatus (Incertae sedis) across the Paleocene–Eocene thermal maximum in ocean drilling program holes 690B and 1209B. *Marine Micropaleontology*, *67*, 239–254. https://doi.org/10.1016/j.marmicro.2008.01.010

Triantaphyllou, M. V., Baumann, K. H., Karatsolis, B. T., Dimiza, M. D., Psarra, S., Skampa, E., et al. (2018). Coccolithophore community response along a natural $CO_2$ gradient off Methana (SW Saronikos Gulf, Greece, NE Mediterranean). *PloS One*, *13*, 1–21. https://doi.org/10.1371/journal.pone.0200012

Troelstra, S. R., Van der Poel, H. M., Huisman, C. H. A., Geerlings, L. P. A., & Dronkert, H. (1980). Paleoecological changes in the latest Miocene of the Sorbas Basin, S.E. Spain. *Géologie Méditerranéenne*, *8*, 115–125. https://doi.org/10.3406/geolm.1980.1132

Urbanek, A. (1993). Biotic crises in the history of Upper Silurian graptoloids: A palaeobiological model. *Historical Biology*, *7*, 29–50. https://doi.org/10.1080/10292389309380442

van de Poel, H. M. (1992). Foraminiferal biostratigraphy of the Carboneras-Nijar Basin. *Scripta Geolica*, *102*, 1–32.

Vasiliev, I., Karakitsios, V., Bouloubassi, I., Agiadi, K., Kontakiotis, G., Antonarakou, A., et al. (2019). Large sea surface temperature, salinity, and productivity-preservation changes preceding the onset of the Messinian Salinity Crisis in the eastern Mediterranean Sea. *Paleoceanography and Paleoclimatology*, *34*, 182–202. https://doi.org/10.1029/2018pa003438

Violanti, D., Lozar, F., Dela Pierre, F., Natalicchio, M., Bernardi, E., Clari, P., et al. (2013). Stress tolerant microfossils of a Messinian succession from the northern Mediterranean basin (Pollenzo section, Piedmont, Northwestern Italy). *Bollettino della Società Paleontologica Italiana*, *52*(1), 45–255. https://doi.org/10.1016/j.palaeo.2011.07.017

Watabe, N., & Wilbur, K. M. (1966). Effects of temperature on growth, calcification, and coccolith form in *Coccolithus huxleyi* (Coccolithineae). *Limnology and Oceanography*, *11*, 567–575. https://doi.org/10.4319/lo.1966.11.4.0567

Yáñez-Arancibia, A., & Day, J. W. (2005). *Ecosystem functioning: The basis for sustainable management of Terminos Lagoon, Campeche, México* (p. 77). Institute of Ecology A.C. https://doi.org/10.1016/j.ecoleng.2013.03.007

Young, J. R., Bown, P. R., & Lees, J. A. (2017). *Nannotax3 website*. International Nannoplankton Association. https://doi.org/10.1016/s0967-0645(00)00003-5

Young, J. R., & Ziveri, P. (2000). Calculation of coccolith volume and it use in calibration of carbonate flux estimates. *Deep Sea Research Part II: Topical Studies in Oceanography*, *47*(9–11), 1679–1700. https://doi.org/10.1016/s0967-0645(00)00003-5

Zeebe, R. E., Ridgwell, A., & Zachos, J. C. (2016). Anthropogenic carbon release rate unprecedented during the past 66 million years. *Nature Geoscience*, *9*(4), 325–329. https://doi.org/10.1038/ngeo2681

Ziveri, P., De Bernardi, B., Baumann, K.-H., Stoll, H. M., & Mortyn, P. G. (2007). Sinking of coccolith carbonate and potential contribution to organic carbon ballasting in the deep ocean. *Deep-Sea Research Part II: Topical Studies in Oceanography*, *54*, 659–675. https://doi.org/10.1016/j.dsr2.2007.01.006

Ziveri, P., Passaro, M., Incarbona, A., Milazzo, M., Rodolfo-Metalpa, R., & Hall-Spencer, J. M. (2014). Decline in coccolithophore diversity and impact on coccolith morphogenesis along a natural $CO_2$ gradient. *The Biological Bulletin*, *226*(3), 282–290. https://doi.org/10.1086/bblv226n3p282

Zondervan, I. (2007). The effects of light, macronutrients, trace metals and CO2 on the production of calcium carbonate and organic carbon in coccolithophores—A review. *Deep Sea Research Part II: Topical Studies in Oceanography*, *54*, 521–537. https://doi.org/10.1016/j.dsr2.2006.12.004

## Reference From the Supporting Information

Gibbs, S., Shackleton, N., & Young, J. R. (2004). Orbitally forced climate signals in mid-Pliocene nannofossil assemblages. *Marine Micropaleontology*, *51*, 39–56. https://doi.org/10.1016/j.marmicro.2003.09.002